AWARD NUMBER: W81XWH-14-1-0326

TITLE: Overcoming Endocrine Resistance by Targeting ER/FoxA1/IL-8 Axis

PRINCIPAL INVESTIGATOR: Xiaoyong Fu

CONTRACTING ORGANIZATION:

Baylor College of
Medicine a Houston, TX
77030-3411

REPORT DATE: October 2015

TYPE OF REPORT: Annual

PREPARED FOR: U.S. Army Medical Research and Materiel Command
Fort Detrick, Maryland 21702-5012

REPORT DOCUMENTATION PAGE

Form Approved
OMB No. 0704-0188

1. REPORT DATE	2. REPORT TYPE	3. DATES COVERED
October 2015	Annual	30 Sep 2014 –29 Sep 2015

4. TITLE AND SUBTITLE

Overcoming Endocrine Resistance by Targeting ER/FoxA1/IL-8 Axis

5a. CONTRACT NUMBER

5b. GRANT NUMBER
W81XWH-14-1-0326

5c. PROGRAM ELEMENT NUMBER

6. AUTHOR(S)

Xiaoyong Fu, Rinath Jeselsohn, Resel Pereira, Emporia F. Hollingsworth, Chad J. Creighton, Fugen Li, Martin Shea, Agostina Nardone, Tao Wang, Laura M. Heiser, Pavana Anur, Nicholas Wang, Catie Grasso, Paul Spellman, Carolina Gutierrez, Dolores Lopez-Terrada, Susan G. Hilsenbeck, Joe W. Gray, Myles Brown, C. Kent Osborne & Rachel Schiff

E-Mail: xiaoyonf@bcm.edu

5d. PROJECT NUMBER

5e. TASK NUMBER

5f. WORK UNIT NUMBER

7. PERFORMING ORGANIZATION NAME(S) AND ADDRESS(ES)

Baylor College of Medicine
One Baylor Plaza
Houston, TX 77030-3411

8. PERFORMING ORGANIZATION REPORT NUMBER

9. SPONSORING / MONITORING AGENCY NAME(S) AND ADDRESS(ES)

U.S. Army Medical Research and Materiel Command
Fort Detrick, Maryland 21702-5012

10. SPONSOR/MONITOR'S ACRONYM(S)

11. SPONSOR/MONITOR'S REPORT NUMBER(S)

12. DISTRIBUTION / AVAILABILITY STATEMENT

Approved for Public Release; Distribution Unlimited

13. SUPPLEMENTARY NOTES

14. ABSTRACT

Endocrine resistant (Endo-R) breast cancer remains challenging for both clinical management and mechanistic understanding. We have developed and characterized a large panel of preclinical Endo-R cell models at multi-omics levels. Preliminary data revealed a novel ER/FOXA1/IL-8 axis as potential therapeutic targets to overcome endocrine resistance. In this 1st year funded study, we focused on the determination of this axis alteration in our Endo-R cell models and the investigation of the role of ER/FOXA1 in IL-8 regulation in endocrine resistance. We further applied genome-wide FOXA1 ChIP-Seq and integrative analysis to understand the mechanistic role of increased FOXA1 in ligand-independent ER transcriptional reprogramming. Our major findings are: 1) *FOXA1* gene amplification exists in two independently developed MCF7-TamR models (L and RN), but not in other Endo-R cell models; 2) FOXA1 and IL-8 expression at either mRNA or protein levels was increased in multiple Endo-R cell models; 3) FOXA1/IL-8 up-regulation was also found in xenograft tumors resistant to endocrine therapy; 4) FOXA1 or ER knockdown decreased the expression of IL-8 but not other cytokines in TamR cells; 5) FOXA1 overexpression in P cells induced multiple cytokines including IL-8 expression in an ER-dependent manner, and a gene signature associated with cell migration and angiogenesis, and decreased response to estrogen; 6) Cistromic profiling suggested the direct binding and regulation of IL-8 by ER/FOXA1. These data substantiate the critical role of ER/FOXA1/IL-8 axis in endocrine resistance, and lay a solid foundation for further translational study in the following years.

15. SUBJECT TERMS

FOXA1, gene amplification, estrogen receptor, interlukin-8, cytokine, transcriptional reprogramming, endocrine resistance

16. SECURITY CLASSIFICATION OF:			17. LIMITATION OF ABSTRACT	18. NUMBER OF PAGES	19a. NAME OF RESPONSIBLE PERSON
a. REPORT	b. ABSTRACT	c. THIS PAGE			USAMRMC
Unclassified	Unclassified	Unclassified	Unclassified	47	19b. TELEPHONE NUMBER *(include area code)*

Standard Form 298 (Rev. 8-98)
Prescribed by ANSI Std. Z39.18

Table of Contents

INTRODUCTION

Approximately 75% of breast cancers express the hormone estrogen receptor α (ER). As a critical determinant in estrogen response and oncogenic driver for ER-positive breast cancer, ER promotes cancer cell proliferation, survival, and metastasis. Successful endocrine therapy targets the ER pathway by inhibiting estrogen synthesis with aromatase inhibitors, blocking ER with selective ER modulators (such as tamoxifen), or eliminating ER with selective ER degraders (such as fulvestrant). However, in ER-positive (+) patients with metastatic disease, more than 50% of patients fail to respond to first-line therapy due to *de novo* resistance, and all patients who do respond eventually relapse and die due to acquired resistance. The mechanism of endocrine resistance has been poorly understood. Our subject in this study is endocrine-resistant (Endo-R) ER+ breast cancer disease. Through integrated approach built on multi-omics platforms including next-generation sequencing of a large panel of our established endocrine-resistant cell models, we previously identified a novel ER/FOXA1/IL-8 signaling axis in our Endo-R cell models. By completing this DoD funded study, we hope to better understand the mechanism of endocrine resistance driven by the alterations of the ER/FOXA1/IL-8 axis, and further develop novel therapeutic approach to target this axis to overcome endocrine resistance and improve patient outcome. The scope of this study is covering both molecular and cellular biology, and integrated bioinformatics analysis of multi-omics data generated from both *in vitro* cell line and *in vivo* xenograft mouse models.

KEYWORDS

FOXA1, gene amplification, estrogen receptor, interlukin-8, cytokine, transcriptional reprogramming, endocrine resistance, xenograft tumor, gene signature, RNA-Seq, ChIP-Seq, multi-omics, integrative analysis

ACCOMPLISHMENTS

1. **Specific Aim 1**: (9/29/14 ~ 9/30/15): Determine alterations in the ER/FOXA1/IL-8 axis in endocrine resistance and the mechanism by which ER/FOXA1 regulates IL-8 and additional cytokines.

   Major Task 1: Determine the alterations of FOXA1 and several cytokines in our large panel of 12 ER+ Endo-R breast cancer cell lines and 3 archived xenograft models. (Months 1-9)

   Status: Completed (100%) and reached the milestone (*5/30/15*)

   Major Task 2: Determine the role of ER/FOXA1 in regulation of cytokines across our Endo-R cell models. (Months 5-12)

   Status: Completed (100%) and reached the milestone (*8/30/15*)

   Major Task 3: Investigate the mechanism of IL-8 upregulation by ER/FOXA1 transcriptional reprogramming in endocrine resistance. (Months 12-18)

   Status: Completed (60%) in advance this 2nd year task (*9/29/15*)

There are no significant changes in approach or methods from the approved SOW.

2. **Major Task 1**

   Subtask 1. *Measure DNA copy-number alteration (CNA) of FOXA1 by using FISH/genomic PCR amplification assays.* In collaboration with Dr. Dolores Lopez-Terrada, from the Cytogenetics Core at Texas Children's Hospital, we developed a specific *FOXA1* FISH assay that works on both cell and tissue slides. High quality and reliability of FISH signal depend on the sensitivity and specificity of hybridizing probes. In order to achieve better results, we first validated two labelled probes from different BAC clones giving rise to clear and discernable *FOXA1*

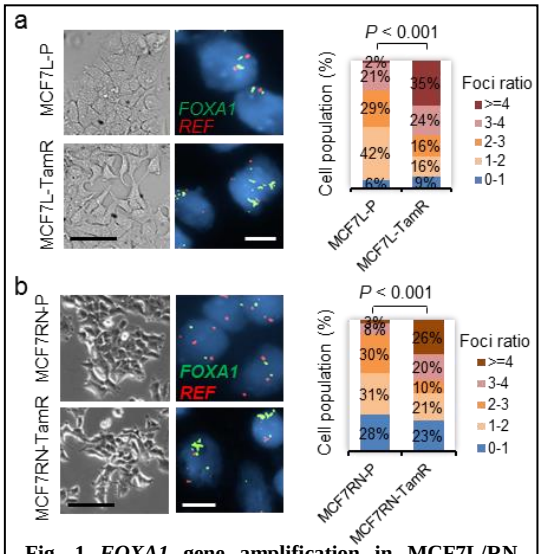

Fig. 1 *FOXA1* gene amplification in MCF7L/RN TamR models. FISH assay showed *FOXA1* gene amplification in both (**a**) MCF7L-TamR and (**b**) MCF7RN-TamR models compared to their P cells. Quantification of the cell populations with different *FOXA1 vs.* chromosome reference (*REF*) foci ratio were shown in the right panel. Scale bars, 100 μm (bright field) and 20 μm (FISH).

foci signals in metaphase chromosomes, along with one reference probe to hybridize a region close to the centromere of chromosome 14, where no aberrations were found in normal breast cancer cells. Then, after labelling for individual probes we mixed these three to make a combo for hybridization. Comparing to a single probe, this combo produces crystal brightness in our *FOXA1*-FISH slides that are easy for following quantification. Using this assay, we measured *FOXA1* amplification at single cell level in two independently developed MCF7 (L and RN) Endo-R models. *FOXA1* amplified cell population (foci ratio ≥4) was highly enriched in tamoxifen-resistant (TamR) than in endocrine-sensitive parental (P) cells in both MCF7L/RN models (**Fig. 1**), in consistence with our previous Exome-Seq data showing *FOXA1* gene amplification in these TamR but not estrogen deprivation-resistant (EDR) cells. Furthermore, we applied a *FOXA1* genomic PCR (gPCR) amplification assay to determine the *FOXA1* CNA across five different Endo-R cell models we have established. In addition to the two MCF7 TamR models, BT474-TamR, another ER+ Endo-R cell model, showed increased FOXA1 CN than that in BT474-P cells (**Fig. 2**). No *FOXA1* amplification was found in ZR75-1 and 600MPE Endo-R cell models. Of note, in accordance to the small *FOXA1*-amplified population found in MCF7-L/RN P cells by FISH, *FOXA1*-CN is increased in both P cells than the normal mammary gland MCF10A cells in gPCR assay, suggesting that some level of *FOXA1* CN-gain (CNG) may preexist in the P cells even before developing endocrine resistance. Since we will work on human samples using this *FOXA1* FISH assay as described in the 3rd year Aim 3 in SOW, we submitted a research protocol related to this study to our institute's IRB and got approved in 12/8/2014 and successfully renewed in August this year (H-35791). We also got an exempt notice for further review requirement from DoD HRPO (A-18414), since this proposed study only relates to tissue/data analysis and won't involve human subjects determination.

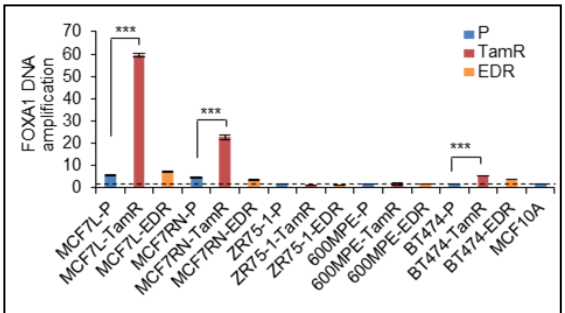

Fig. 2 *FOXA1*-CN measurement by gPCR in multiple preclinical Endo-R cell models. *FOXA1*-CN values were normalized to the normal diploid MCF10A cell line (CN = 2 as indicated by a dashed line). *** $P < 0.001$, unpaired two-sided *t*-test.

Subtask 2. *Measure mRNA levels of ER, FOXA1, and IL-8 by using q-RT-PCR and ISH assays.* In the past four years, we have developed a large panel of ER+ breast cancer preclinical Endo-R cell models. Most of these models include both TamR and EDR derivatives along with the P cell lines. We applied qRT-PCR assay to measure the mRNA levels of FOXA1, ER, and IL-8 in these models. We found that FOXA1 mRNA levels significantly increased in both TamR and EDR cells compared to the P cells in MCF7RN, ZR75-1, 600MPE models; increased in TamR but not EDR cells in MCF7L model; no change in MDA-MB-415 model; and decreased in both TamR and EDR cells in T47D model (**Fig. 3a**). In contrast, ER mRNA levels were decreased in TamR compared to P cells in both MCF7L and MCF7RN models; decreased in both TamR and EDR cells in ZR75-1 and T47D models; and increased in 600MPE and MDA415 Endo-R models (**Fig. 3b**). Since our hypothesis is that IL-8 expression in Endo-R cells is regulated by increased FOXA1, we measured the IL-8 mRNA

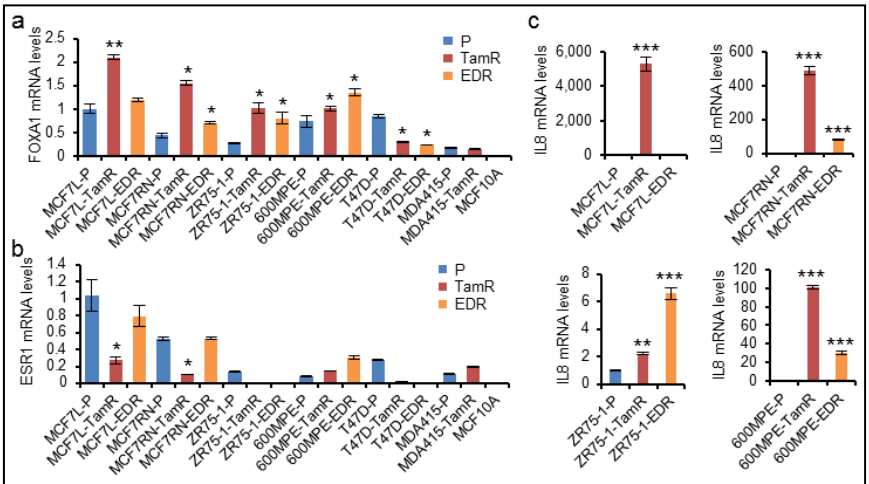

Fig. 3 The mRNA levels of FOXA1, ER, and IL-8 in multiple Endo-R cell models. (**a**) and (**b**), FOXA1 and ER mRNA levels in all measured cell models were normalized to the levels in MCF7L-P cells (set as 1). (**c**) IL-8 mRNA levels were measured in 4 Endo-R models with up-regulated FOXA1. * $P < 0.05$, ** $P < 0.01$, *** $P < 0.001$, unpaired two-sided *t*-test comparing Endo-R cells to P cells in each model.

levels in the 4 Endo-R cell models with up-regulated FOXA1. Indeed, the IL-8 mRNA levels were significantly induced in Endo-R cells of these 4 models except the EDR cells in MCF7L model (**Fig. 3c**), which is consistent with the FOXA1 mRNA changes in these models. Since IL-8 mRNA was reported to be unstable, we did not use the assay of IL-8 *in situ* hybridization (ISH), which being proposed as an alternative method to specifically detect IL-8 expressing cells in human tissue samples. Instead, we have developed a sensitive IL-8 immunohistochemistry (IHC) protocol for this purpose as shown below.

Subtask 3. *Measure protein levels of ER, FOXA1, and IL-8 using Western blotting, antibody array, ELISA, and IHC.* We measured ER and FOXA1 protein levels by Western blotting in multiple preclinical Endo-R cell models. ER expression was maintained in MCF7L, MCF7RN, 600MPE, and MDA-MB-415 Endo-R models, whereas lost in both ZR75-1 and T47D Endo-R cells compared to their P cells (**Fig. 4a**). These data are partially consistent with the results of mRNA expression measured by qRT-PCR assay. FOXA1 protein levels were increased in TamR cells of both MCF7L and RN models, and in TamR and EDR cells of ZR75-1 model; remain the same in 600MPE model; but decreased in T47D Endo-R cells, which are also consistent to the changes of mRNA levels in these cells. Since IL-8 is a small molecular weight (10 kDa) protein that is hardly detected by conventional Western blotting, we applied two other protein measurement assays. We used the cytokine antibody protein array to measure the secreted IL-8. We found highly upregulated IL-8 along with some other cytokines (e.g., TGF-β) in the conditioned media from MCF7L-TamR compared to the P cells (**Fig. 4b**). We also used the IL-8 ELISA kit to determine the IL-8 levels in the conditioned media from multiple Endo-R models. In addition to the MCF7L/RN TamR cells, 600MPE-TamR and EDR cells secreted more IL-8 in culture media than their P cells (**Fig. 4c**). There were no changes of IL-8 amount in conditioned media from MCF7L/RN EDR cells, and slight increase in Endo-R (TamR and EDR) cells of ZR75-1 model. In order to measure proteins in tissue samples, we optimized the FOXA1 and IL-8 IHC protocol using an indexed cell pellet array, which integrated positive and negative control of cell pellets through overexpression or knockdown of target genes. We then performed IHC assay using archived FFPE samples of our previously developed MCF7L Endo-R xenograft tumors. Compared to the tumors under E2 treatment, TamR tumors showed significantly higher expression levels of both FOXA1 and IL-8; EDR tumors showed significantly increased levels of ER, FOXA1, and IL-8 (**Fig. 5a** and **b**). Overall, these data further demonstrated the upregulation of ER/FOXA1/IL-8 axis in both *in vitro* cell and *in vivo* xenograft Endo-R models.

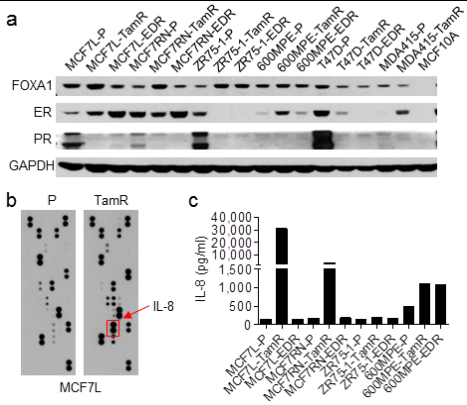

Fig. 4 The protein levels of FOXA1, ER, and IL-8 in multiple Endo-R cell models. (**a**) Western blots showing the protein changes across 6 Endo-R cell models. (**b**) Cytokine antibody array measurement of the secreted proteins in conditioned media from MCF7L model. (**c**) ELISA measurement of IL-8 protein in conditioned media from 4 Endo-R models.

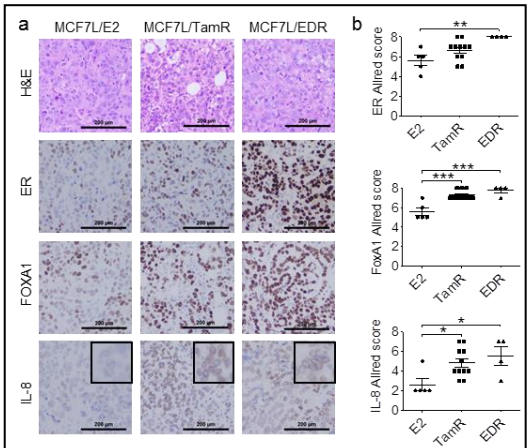

Fig. 5 Protein expression in MCF7L xenograft tumors. (**a**) H&E and IHC of ER, FOXA1, and IL-8 in MCF7L xenograft tumors treated with E2, and Endo-R tumors (TamR and EDR). Scale bar, 200 μm. (**b**) Scatter dot plots of Allred score of staining in (a). Data represent means ± SEM. * $P < 0.05$, ** $P < 0.01$, *** $P < 0.001$, unpaired two-sided *t*-test.

In summary, we completed 100% and reached the milestone of Major Task 1: *we confirmed the alterations of FOXA1 and IL-8 at all levels (DNA, RNA, and protein) across our large panel of Endo-R cell and xenograft models.*

Major Task 2

Subtask 1. *Verify whether FOXA1 and ER are responsible for the upregulation of IL-8 and other cytokines in Endo-R cells by siRNA knockdown assay.* We verified the ER and FOXA1 knockdown efficiency in MCF7L and 600MPE models by both Western blots and qRT-PCR assays (**Fig. 6**). ER or FOXA1 knockdown in the TamR cells from MCF7L and 600MPE models, where IL-8 was highly upregulated compared to P cells (see above), significantly decreased IL-8 mRNA levels in both TamR models, with more effect in the MCF7L-TamR cells with FOXA1 knockdown (**Fig. 7a** and **b**). Similar results were obtained using a second siRNA sequence of ER or FOXA1 in MCF7L-TamR model. We performed next-generation RNA-Seq of MCF7L-TamR cells with knockdown of non-specific (N.S.) control, FOXA1, or ER. Analysis of the RNA-Seq data revealed that the expression of other cytokines (VEGFC, TGFB1, CXCL17, BMP2, and BMP7), which were upregulated in MCF7L-TamR *vs*. P cells shown by our previous RNA-Seq data, cannot be suppressed by either FOXA1 or ER knockdown (**Fig. 7c**), suggesting other mechanism in regulating these genes in TamR cells. Therefore, we concluded that FOXA1 and ER are responsible specifically for the upregulation of IL-8, but not other upregulated cytokines identified in TamR cells.

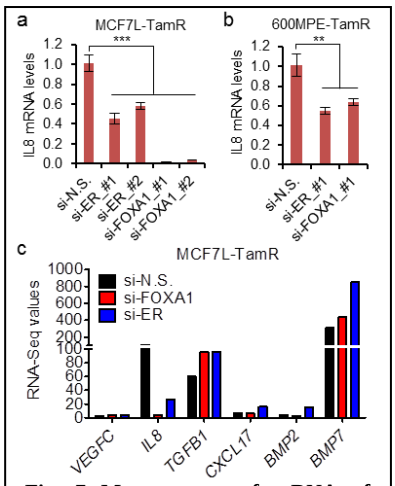

Fig. 7 Measurement of mRNA of cytokines in TamR cells upon ER or FOXA1 knockdown. IL-8 mRNA levels by qRT-PCR in (**a**) MCF7L-TamR and (**b**) 600MPE-TamR cells with ER or FOXA1 knockdown. (**c**) RNA-Seq data showing mRNA levels of several cytokines in MCF7L-TamR cells upon ER or FOXA1 knockdown. ** $P < 0.01$, *** $P < 0.001$, unpaired two-sided *t*-test.

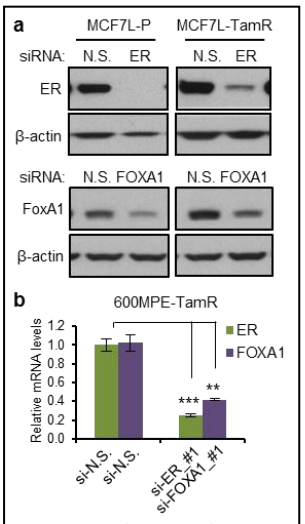

Fig. 6 Verification of siRNA knockdown. (**a**) Western blots and (**b**) qRT-PCR of protein and mRNA of ER and FOXA1 in cells with knockdown. *** $P < 0.001$, unpaired two-sided *t*-test.

Subtask 2. *Determine whether upregulated FOXA1 induces IL-8 and other cytokines in parental ER+ breast cancer cell lines by using an inducible cDNA overexpression system.* We constructed a doxycycline (Dox)-inducible FOXA1 overexpression system in MCF7L-P cells. We performed RNA-Seq of extracted RNA from MCF7L-FOXA1 ± Dox cells. RNA-Seq analysis revealed a total of 440 genes up-regulated and 217 genes down-regulated (|Gfold| > 1.5) in +Dox *vs*. –Dox cells (**Fig. 8a**). Functional annotation of these up-regulated genes in DAVID showed a robust enrichment of GO terms that included cell motion and migration, response to hypoxia, and blood vessel development (**Fig. 8b**). Within the down-regulated genes, the most enriched GO term was response to estrogen, suggesting the reduction of ligand-dependent ER transcriptional activity in this model. Focusing on the cytokines that were up-regulated in TamR *vs*. P cells, only the expression of TGFB1 and BMP7 together with IL8 was markedly increased in P cells upon FOXA1 overexpression (**Fig. 8c**). Of note, the increased levels of TGFB1 and BMP7 in TamR cells were not reduced by FOXA1 knockdown, suggesting different mechanisms by which FOXA1 regulates these two genes in P *vs*. TamR cells. Since MCF7L-TamR and 600MPE-TamR cells highly express IL-8 that can be

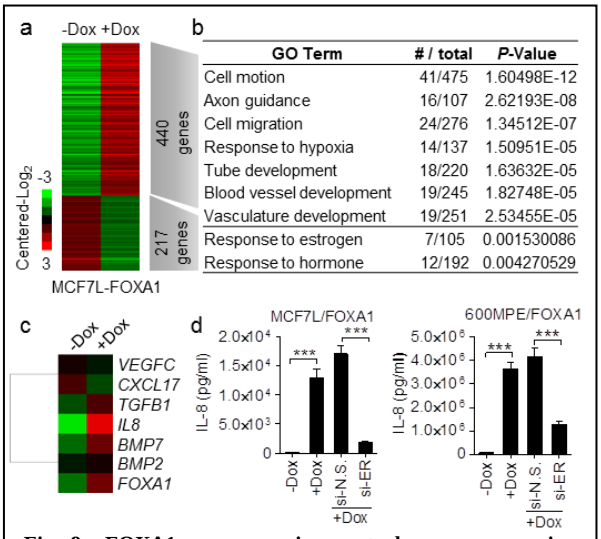

Fig. 8 FOXA1 overexpression perturbs gene expression profile and up-regulates IL-8 in P cells in an ER-dependent manner. **(a)** Heatmap of differentially expressed genes after FOXA1 overexpression in MCF7L/FOXA1 cells. (**b**) The enriched GO terms in DAVID annotation of differential genes. (**c**) Changes of cytokines mRNA in ±Dox cells. (**d**) ELISA of IL8 in media from MCF7L and 600MPE cells with ±FOXA1 overexpression and/or concomitant ER knockdown. *** $P < 0.001$, unpaired two-sided *t*-test.

decreased by ER or FOXA1 knockdown, we asked whether both FOXA1 and ER are required for IL-8 upregulation in P cells upon FOXA1 overexpression. IL-8 ELISA using conditioned media showed that both MCF7L/FOXA1 and 600MPE/FOXA1 cells highly expressed IL-8 upon +Dox, which was suppressed by knockdown of ER (**Fig. 8d**). In summary, these data support the notion that FOXA1, together with ER, is a key regulator for IL-8 expression in endocrine resistance. High level of FOXA1 drives a gene signature associated with cell motion and migration and less response to estrogen, suggesting its potential role in breast cancer Endo-R disease.

In summary, we completed 100% and reached the milestone of Major Task 2: *we determined the relationship between ER/FOXA1 & other cytokines in our large panel of Endo-R cell models.*

Major Task 3

Subtask 1. *Correlate FOXA1 genome-wide binding sites with gene expression profiles in our 3 prioritized Endo-R cell models by using integrative bioinformatics analysis.* In collaboration with Drs. Rinath Jeselsohn and Myles Brown at Dana-Farber Cancer Institute, we performed genome-wide FOXA1 ChIP-Seq in MCF7L-P and MCF7L-TamR cells. We used the Model-based Analysis of ChIP-Seq (MACS) to call peaks and found a total of 37,227 and 53,215 FOXA1 binding events in MCF7L-P and TamR cells, respectively (**Fig. 9a**). There were 21,449 FOXA1 binding sites shared between P and TamR cells, accounting for 58% and 40% of total binding sites in P and TamR cells, respectively. Enriched binding motif analysis revealed the highest enrichment of FOXA1 motif followed by the GATA motif in P cells, and the BCL11A and JUN/FOS motifs in TamR cells, implying the significant FOXA1 binding in both P and TamR cells albeit on different sites (**Fig. 9b**). We further used our previous RNA-Seq data in MCF7L model to integrate FOXA1 ChIP-Seq data. By defining the genes meeting the criteria as 1) highly expressed in TamR *vs*. P cells ($\log_2$(fold) > 1.5, FDR < 0.05); 2) carrying the most abundant FOXA1 binding sites around their gene regions (± 20 kb from transcription start sites) in TamR *vs*. P cells (log10(fold) > 1.5), we identified 27 genes including *IL8* at the top of the list (**Fig. 10**). The enriched GO terms within these top genes included the blood vessel development (*IL8*, *CTGF*, *LOX*, and *ROBO1*), response to wounding (*BMP2*, *CTGF*, *DCBLD2*, *IL8*, and *LOX*), and cell migration (*CTGF*, *IL8*, *NR2F1*, and *ROBO1*), reminiscent of the GO terms enriched in the MCF7L/FOXA1 +Dox cells. Indeed, 4 of these 7 genes (*IL8*, *LOX*, *NR2F1*, and *CTGF*) were highly up-regulated in FOXA1-overexpressing MCF7L-P cells, suggesting FOXA1-dependent regulation of these genes. With a separate research funding, we acquired additional RNA-Seq data in two more Endo-R models (ZR75-1 and 600MPE). Together with MCF7L, we prioritized these 3 models because of the increased FOXA1 and IL-8 expression (mRNA and protein) in their Endo-R *vs*. P cells. We will continue our FOXA1 ChIP-Seq and subsequent integrated approach in these models (first half year of the 2nd funding cycle as stated in SOW) to identify the differentially expressed genes potentially regulated by FOXA1 in Endo-R cells. We realized that this endeavor is actually beyond the scope we aim in this study, but we believe that

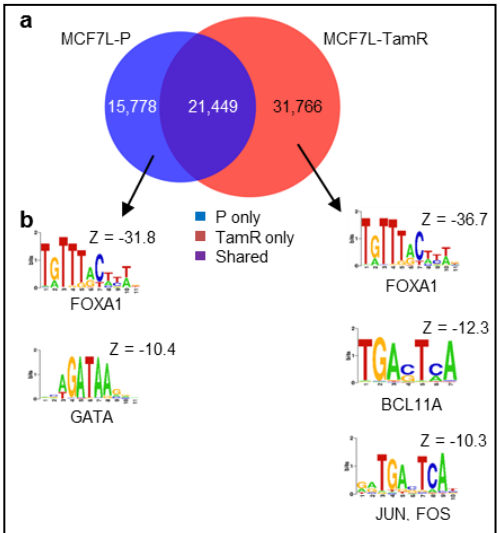

Fig. 9 Cistromic profiling of FOXA1 in MCF7L-P and TamR cells. **(a)** Venn diagram showing the overlap of FOXA1 binding sites between MCF7L-P and TamR cells. (**b**) Motif enrichment analysis of differential FOXA1 binding sites.

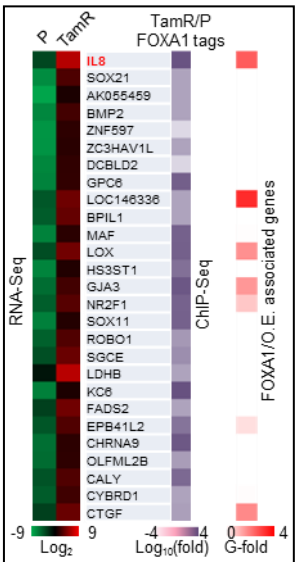

Fig. 10 Integrative analysis revealed *IL8* as a potential target of increased FOXA1 in TamR cells. Heatmap of genes with high expression ratio and FOXA1 binding ratio in TamR *vs*. P cells. Alongside heatmap shows the expression ratio of these genes in MCF7L-FOXA1 +Dox *vs*. -Dox cells.

it will help us to nominate more FOXA1-regulated genes in endocrine resistance as potential targets, and allow us to pursue future funding opportunities.

Subtask 2. *Determine the binding sites and intensity of ER/FOXA1 within the gene regions of several cytokines in our 3 prioritized Endo-R cell models by using ChIP-qPCR.* Using previously published ER ChIP-chip and FOXA1 ChIP-Seq data from Dr. Brown's labs, we identified two potential ER and FOXA1 binding regions around the enhancer and promoter of *IL8* gene (**Fig. 11a**). Interestingly, ER binding to the enhancer region was only seen in ER ChIP-chip data from MCF7 cells treated with EGF but not E2, suggesting that IL8 expression regulated by ER may involve ER activation in an ligand-independent manner. Analysis of our FOXA1 ChIP-Seq data also showed the FOXA1 binding at both enhancer and promoter regions with higher intensity in MCF7L-TamR cells than in P cells (**Fig. 11b**). These binding patterns in P and TamR cells remained same in cells treated with either Tam or estrogen (E2), suggesting that the FOXA1 binding to *IL8* gene is not E2 dependent. We further validated these enhanced FOXA1 binding in MCF7L-TamR *vs.* P cells by using ChIP-qPCR to specifically amplify the regions recognized by FOXA1 (**Fig. 11c**). In addition, we found that the intensity of ER binding in TamR cells was significantly increased at the *IL8* enhancer, where the ER binds in P cells only after EGF treatment (**Fig. 11d**). These data support the notion that IL8 gene is regulated by FOXA1 and ER in Endo-R cells as part of the consequences of ER transcriptional reprogramming activated by growth factor receptor (GFR) signaling in a ligand-independent manner. As described above, we will identify the FOXA1 binding sites around *IL8* gene in additional two Endo-R models (ZR75-1 and 600MPE) when the FOXA1 ChIP-Seq data are available. Meanwhile, since neither ER nor FOXA1 knockdown in MCF7L-TamR cells affected mRNA expression of the group of cytokines in our study other than IL-8 (see above in Fig. 7c), we will explore the possible specificity in Endo-R cell models for the ER/FOXA1 regulated cytokine expression. We will integrate the FOXA1 ChIP-Seq data and the gene expression data (RNA-Seq or qRT-PCR) in Endo-R cells with ER/FOXA1 knockdown. The subject of this project is mainly focusing on the ER/FOXA1/IL-8 axis, but eventually we want to extend these findings to a more general scenario of cytokine involved endocrine resistance by using different Endo-R cell models. Therefore, we expect that this funded study will lay a solid foundation for us to move forward.

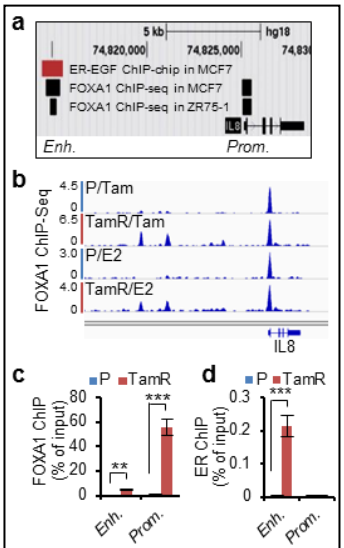

Fig. 11 Enhanced FOXA1 and ER binding in *IL8* gene region in MCF7L-TamR *vs.* P cells. (**a**) Snap shot of genome browser of FOXA1 and ER binding in IL8 gene in MCF7 cells. *Enh.*, enhancer. *Prom.*, promoter. (**b**) Snap shot of FOXA1 continuous binding patterns upstream of IL8 gene in MCF7L-P and TamR cells treated with Tam or E2. (**c**) FOXA1-ChIP and (**d**) ER-ChIP followed by qPCR of binding regions in P and TamR cells. ** $P < 0.01$, *** $P < 0.001$, unpaired two-sided *t*-test.

In summary, we completed in advance 60% of Major Task 3 described in the 2nd year SOW: *We will continue to determine the molecular mechanism by which ER/FOXA1 regulates IL-8 expression through a transcriptional reprogramming in endocrine resistance.*

3. Opportunities for training and professional development

Nothing to Report.

4. Results disseminated to communities of interest

Nothing to Report.

5. Plan to do during the next reporting period to accomplish the goals

In the next funding cycle, we will perform genome-wide ER and FOXA1 ChIP-Seq to further investigate the mechanism of IL-8 upregulation by ER/FOXA1 transcriptional reprogramming in endocrine resistance. We will also investigate the impact of altered FOXA1/IL-8 axis (Dox-inducible overexpression/knockdown

system) on endocrine resistance/sensitivity across our 3-4 prioritized Endo-R cell models. All these experiments will be performed according to the approved SOW.

IMPACT

Nothing to Report.

CHANGES/PROBLEMS

We submitted an animal protocol to the IACUC at Baylor College of Medicine, which covers our designed animal experiments in the SOW. We got this protocol (AN-6577) approved by the IACUC on 8/5/14, and further approved by the USAMRMC ACURO (BC132572) on 3/20/15. Our *in vitro* data from the 1st year Major Task 2 strongly support a role of increased FOXA1 in promoting cell migration and vasculature (Fig. 8). In order to determine the impact of up-regulated FOXA1/IL-8 axis on endocrine sensitivity and/or tumor metastasis in our xenograft mouse model, we modified our protocol and added the procedures of survival surgery and blood collection for IL-8 measurement. These amendments were approved by IACUC on 11/24/14 and 4/27/15, respectively. We further received the approval letter for the protocol amendment from the ACURO on 7/8/15.

PRODUCTS

1. **Publications, conference papers, and presentations**

   Manuscript

   Xiaoyong Fu, Rinath Jeselsohn, Resel Pereira, Emporia F. Hollingsworth, Chad J. Creighton, Fugen Li, Martin Shea, Agostina Nardone, Laura M. Heiser, Pavana Anur, Nicholas Wang, Catie Grasso, Paul Spellman, Anna Tsimelzon, Carolina Gutierrez, Shixia Huang, Dean P. Edwards, Mothaffar F. Rimawi, Dolores Lopez-Terrada, Susan G. Hilsenbeck, Joe W. Gray, Myles Brown, C. Kent Osborne & Rachel Schiff. FOXA1 overexpression mediates endocrine resistance by increasing IL-8 in oestrogen receptor-positive breast cancer. *Nature Communications*, 2015, in preparation.

   Conference presentation

   Xiaoyong Fu, Rinath Jeselsohn, Emporia F. Hollingsworth, Dolores Lopez-Terrada, Chad J. Creighton, Agostina Nardone, Martin Shea, Laura M. Heiser, Pavana Anur, Nicholas Wang, Catie Grasso, Paul Spellman, Carolina Gutierrez, Mothaffar F. Rimawi, Susan G. Hilsenbeck, Joe W. Gray, Myles Brown, C. Kent Osborne, Rachel Schiff. *FOXA1* gene amplification in ER+ breast cancer mediates endocrine resistance by increasing IL-8. Poster discussion at the 37th San Antonio Breast Cancer Symposium, *Cancer Res* 2015, 75; PD6-2.

2. **Websites or other Internet sites**

   Nothing to Report.

3. **Technologies or techniques**

   Nothing to Report.

4. **Inventions, patent applications, and/or licenses**

   Nothing to Report.

5. **Other products**

   RNA-Seq and FOXA1 ChIP-Seq data: from MCF7L/FOXA1 ±Dox cells, and MCF7L-P/TamR cells. We will deposit these data to public Gene Expression Omnibus (GEO) database, during manuscript submission.

   Preclinical breast cancer Endo-R cell models: 600MPE-TamR/EDR and MDA-MB-415-TamR cells

   Dox-inducible FOXA1-overexpressing cell models: MCF7L/FOXA1 and 600MPE/FOXA1 cells

   FOXA1-FISH assay: validated hybridization combo probes, optimized protocol

PARTICIPANTS & OTHER COLLABORATIING ORGANIZATIONS

1. Participants

Name: Xiaoyong Fu
Project Role: Principal Investigator
Nearest person month worked: 10
Contribute to Project: Dr. Fu has overseen this project, coordinated the efforts from collaborators, worked on experimental design, performed the experiments and data analysis, and written the report and manuscript.

Name: Resel Pereira
Project Role: Research Assistant
Nearest person month worked: 12
Contribute to Project: Ms. Pereira has assisted Dr. Fu to perform the experiments and in charge of maintaining our preclinical Endo-R cell models

Name: Susan Hilsenbeck
Project Role: Key personnel
Nearest person month worked: 1
Contribute to Project: Dr. Hilsenbeck has participated in experimental design and performed the biostatistics analysis of experimental results

Name: Chad Creighton
Project Role: Key personnel
Nearest person month worked: 1
Contribute to Project: Dr. Creighton has performed bioinformatics analysis of next-generation sequencing data

Name: Rinath Jeselsohn
Project Role: Key personnel
Nearest person month worked: 1
Contribute to Project: Dr. Jeselsohn has collaborated in the RNA-Seq and ChIP-Seq experiments and data analysis

Name: Rachel Schiff
Project Role: Key personnel
Nearest person month worked: 1
Contribute to Project: Dr. Schiff has collaborated in experimental design and data interpretation.

Name: Tao Wang
Project Role: Non-Key personnel
Nearest person month worked: 1
Contribute to Project: Dr. Wang has assisted in animal experimental design and data analysis of *in vivo* model.

Name: Carolina Gutierrez
Project Role: Non-Key personnel, in replace to Alejandro Contreras, who moved out of Baylor
Nearest person month worked: 1
Contribute to Project: Dr. Gutierrez has assisted in development of FOXA1/IL-8 IHC and data analysis

Name: Emporia Hollingsworth
Project Role: Collaborator
Nearest person month worked: 2
Contribute to Project: Ms. Hollingsworth has performed the *FOXA1* FISH assay and data analysis

Name: Dolores Lopez-Terrada
Project Role: Collaborator
Nearest person month worked: 1
Contribute to Project: Dr. Lopez-Terrada has assisted in FISH data analysis

Name: Agostina Nardone
Project Role: Collaborator
Nearest person month worked: 2
Contribute to Project: Dr. Nardone has assisted in animal experiment.

Name: Martin Shea
Project Role: Collaborator
Nearest person month worked: 3
Contribute to Project: Dr. Shea has assisted in animal experiment.

Name: Fugen Li
Project Role: Collaborator
Nearest person month worked: 1
Contribute to Project: Dr. Li has performed the bioinformatics analysis of RNA-Seq and ChIP-Seq data.

Name: Laura Heiser
Project Role: Collaborator
Nearest person month worked: 1
Contribute to Project: Dr. Heiser has performed in the Exome-Seq of Endo-R cell models.

Name: Pavana Anur
Project Role: Collaborator
Nearest person month worked: 1
Contribute to Project: Dr. Anur has assisted in the analysis of Exome-Seq data

Name: Nicholas Wang
Project Role: Collaborator
Nearest person month worked: 1
Contribute to Project: Dr. Wang has assisted in the Exome-Seq data analysis

Name: Catie Grasso
Project Role: Collaborator
Nearest person month worked: 1
Contribute to Project: Dr. Grasso has assisted in the next-generation sequencing data analysis

Name: Paul Spellman
Project Role: Collaborator
Nearest person month worked: 1
Contribute to Project: Dr. Spellman has assisted in the Exome-Seq data analysis

Name: Joe Gray
Project Role: Collaborator
Nearest person month worked: 1
Contribute to Project: Dr. Gray has assisted in the Exome-Seq data analysis

Name: Myles Brown
Project Role: Collaborator
Nearest person month worked: 1
Contribute to Project: Dr. Brown has assisted in ChIP-Seq experimental design and data analysis

Name: C. Kent Osborne
Project Role: Collaborator
Nearest person month worked: 1
Contribute to Project: Dr. Osborne has participated in experimental design and data analysis

2. **There are no changes in the active other support of the PI or key personnel.**
3. **Other organizations**

Organization Name: Texas Children's Hospital
Location of Organization: Houston, Texas
Partner's contribution to the project: Collaboration in the *FOXA1* FISH assay and data analysis

Organization Name: Dana-Farber Cancer Institute
Location of Organization: Boston, Massachusetts
Partner's contribution to the project: Collaboration in the FOXA1 ChIP-Seq and data analysis

SPECIAL REPORTING REQUIREMENTS

None

APPENDICES

1. **Copies of manuscript:**
   Xiaoyong Fu, Rinath Jeselsohn, Resel Pereira, Emporia F. Hollingsworth, Chad J. Creighton, Fugen Li, Martin Shea, Agostina Nardone, Laura M. Heiser, Pavana Anur, Nicholas Wang, Catie Grasso, Paul Spellman, Anna Tsimelzon, Carolina Gutierrez, Shixia Huang, Dean P. Edwards, Mothaffar F. Rimawi, Dolores Lopez-Terrada, Susan G. Hilsenbeck, Joe W. Gray, Myles Brown, C. Kent Osborne & Rachel Schiff. FOXA1 overexpression mediates endocrine resistance by increasing IL-8 in oestrogen receptor-positive breast cancer. *Nature Communications*, 2015, in preparation.

2. **Abstract of Poster Discussion in San Antonio Breast Cancer Symposium (SABCS, 2014):**
   Xiaoyong Fu, Rinath Jeselsohn, Emporia F. Hollingsworth, Dolores Lopez-Terrada, Chad J. Creighton, Agostina Nardone, Martin Shea, Laura M. Heiser, Pavana Anur, Nicholas Wang, Catie Grasso, Paul Spellman, Carolina Gutierrez, Mothaffar F. Rimawi, Susan G. Hilsenbeck, Joe W. Gray, Myles Brown, C. Kent Osborne, Rachel Schiff. *FoxA1* gene amplification in ER+ breast cancer mediates endocrine resistance by increasing IL-8. Poster discussion at the 37th San Antonio Breast Cancer Symposium, *Cancer Res* 2015, 75; PD6-2.

Journal submission: ***Nature Communications***
Main body word limit: 5,000; Abstract word limit: 150

FOXA1 overexpression mediates endocrine resistance by increasing IL-8 in oestrogen receptor-positive breast cancer

Xiaoyong Fu[1,2,3], Rinath Jeselsohn[6], Resel Pereira[1,2,3], Emporia F. Hollingsworth[5], Chad J. Creighton[2,4], Fugen Li[6], Martin Shea[1,2,4], Agostina Nardone[1,2,4], Carmine De Angelis[1,2,4], Laura M. Heiser[7], Pavana Anur[8], Nicholas Wang[7], Catie Grasso[7], Paul Spellman[8], Obi Griffith[9], Anna Tsimelzon[1,2], Carolina Gutierrez[5], Shixia Huang[3], Dean P. Edwards[3], Mothaffar F. Rimawi[1,2,4], Dolores Lopez-Terrada[5], Susan G. Hilsenbeck[1,2,4], Joe W. Gray[7], Myles Brown[6], C. Kent Osborne[1,2,3,4] & Rachel Schiff[1,2,3,4]

[1]Lester and Sue Smith Breast Center, [2]Dan L. Duncan Cancer Center, and Departments of [3]Molecular and Cellular Biology, [4]Medicine, and [5]Pathology, Baylor College of Medicine, Houston, Texas 77030, USA. [6]Dana-Farber Cancer Institute, Harvard Medical School, Boston, Massachusetts 02215, USA. Departments of [7]Biomedical Engineering, and [8]Molecular and Medical Genetics, Oregon Health and Science University, Portland, Oregon 97239, USA. [9]McDonnell Genome Institute, Washington University, St. Louis, Missouri 63108, USA.

FOXA1 is a pioneer factor of oestrogen receptor α (ER)-chromatin binding and function, yet its aberration in endocrine-resistant (Endo-R) breast cancer is unknown. Here, we report preclinical evidence of the role of FOXA1 in Endo-R breast cancer and its clinical significance. FOXA1 is gene amplified and/or overexpressed in Endo-R derivatives in several preclinical breast cancer models. Induced FOXA1 triggers oncogenic gene signatures and proteomic profiles highly associated with endocrine resistance. *FOXA1* copy number gain (CNG)-associated gene signature predicts poor disease-free survival in patients with ER$^+$ tumours. Integrated omics data revealed interleukin (IL)-8 as one of the most perturbed genes under FOXA1 and ER regulation in tamoxifen-resistant (TamR) cells. IL-8 knockdown inhibits TamR cell growth and invasion, and partly attenuates the effect of overexpressed FOXA1 in ER$^+$ breast cancer cells. Our study highlights a novel stoichiometric role of FOXA1 via IL-8 signaling as a potential therapeutic target in FOXA1-overexpressing ER$^+$ tumours.

About 75% of breast cancers express oestrogen receptor α (ER), which is a strong driver and therapeutic target for ER-positive ($^+$) tumours. Endocrine therapy with aromatase inhibitors lowers the level of oestrogen;

selective ER modulators like tamoxifen (Tam) bind to and block ER; and downregulators like fulvestrant (Ful) bind to ER and induce its degradation. Endocrine therapy prolongs disease-free and overall survival when used in the adjuvant setting and induces sustained remission in the metastatic setting with ER^+ disease. Despite the overall success of endocrine therapy, more than 50% of patients with metastatic disease fail to respond. Most of the patients, who initially respond, eventually relapse and die from acquired resistance[1, 2]. Although there are many causes for resistance, the most predominant mechanisms include altered ER signaling and interactions between ER and its co-regulators. These alterations allow adaptation from ligand-dependent to ligand-independent ER activation, which is further triggered by cross-talk with growth factor receptor (GFR) signaling pathways[3-6]. However, the key mediators of ER transcriptional reprogramming in promoting endocrine-resistant (Endo-R) breast cancer remain poorly understood.

Recently, a potential role of the forkhead-box protein FOXA1 has been suggested in mediating endocrine resistance in breast cancer. FOXA1 is termed a "pioneer factor" because it binds to the highly compacted or "closed" chromatin via a domain similar to that of linker histones[7] and through its C-terminal domain makes these genomic regions more accessible to other transcription factors, such as ER[8], progesterone receptor (PR)[9], and androgen receptor (AR)[10]. As such, FOXA1 has a key role in demarcating the tissue-specific binding sites of these nuclear receptors[11]. Together with ER, FOXA1 contributes to the pattern of gene transcription that induces luminal cell differentiation[12] and represses the basal phenotype[13]. In breast cancer, however, there are conflicting reports regarding FOXA1 expression in predicting outcomes of ER^+ patients and regarding its role in tumour progression in patients treated with endocrine therapy. For example, the expression of FOXA1 correlates with ER positivity[14]. Similar to ER, FOXA1 is associated with luminal subtype and good prognosis in breast cancer[15-17]. However, FOXA1 and ER are also found to be co-expressed at high levels in breast cancer metastases that are resistant to endocrine therapy[18], suggesting a different role in ER^+ metastatic and/or resistant disease. A recent study in endometrial cancer has shown increasing level of FOXA1 in metastases, even though the high levels of FOXA1 in primary tumours were associated with good outcome[19]. At the molecular level, genome-wide mapping of *cis*-regulatory elements (cistromes) has shown that the FOXA1-binding motif is enriched in a distinct ER cistrome identified in ER^+ primary tumours from patients

that are likely to relapse, suggesting a functional link of FOXA1 with aggressive ER^+ disease[18]. These contradictory findings on FOXA1 in early and late stages of tumours suggest a potentially dynamic perturbation of FOXA1 during disease progression. However, it remains unclear how FOXA1 is engaged in ER transcriptional reprogramming in Endo-R breast cancer, and whether there is any aberration of FOXA1 that contributes to this process.

The aim of this study was to evaluate the role of FOXA1 in mediating endocrine resistance in ER^+ breast cancer using a panel of preclinical Endo-R breast cancer cell models, publicly available clinical data, and functional studies. FOXA1 expression was increased in Endo-R derivatives compared to ER^+ parental (P) breast cancer cells of various preclinical models. Induced overexpression of FOXA1 in the P cells elicited gene signatures and proteomic profiles associated with multiple oncogenic pathways and endocrine resistance. *FOXA1* copy number gain (CNG)-associated gene signature derived from ER^+ breast tumours predicted poor outcome in patients with ER^+ but not ER^- disease. Integrative analysis of cistromic and RNA-sequencing (Seq) data suggested that interleukin (IL)-8 might serve as an important mediator of FOXA1/ER transcriptional reprogramming to convey Endo-R cell growth and invasion. We propose that targeting IL-8 signaling is a promising strategy to treat ER^+ tumours with high levels of FOXA1.

Results

***FOXA1* gene amplification is associated with Tam resistance in ER^+ breast cancer preclinical models.** All our established Endo-R cell models showed stable phenotype of sustained cell growth in the presence of oestrogen-deprivation (ED) or Tam (**Supplementary Fig. S1**). Two MCF7 Endo-R cell models were independently developed from the ER^+ breast cancer MCF7- L[20] and RN[21] lines. The genomic region (14q21.1) encompassing only the *FOXA1* gene had the highest focal amplification ratio in Tam-resistant (TamR) derivatives compared to P cells in both MCF7(L/RN) models (**Fig. 1a** and **b**), which was validated using a genomic polymerase chain reaction (gPCR) assay (**Supplementary Fig. S2a**). The *FOXA1* gene amplification was selective to the MCF7(L/RN)-TamR but not the ED resistant (EDR) derivatives. Furthermore, at a single cell level there was a highly enriched cell population with *FOXA1* amplification (*FOXA1 vs*. chromosome reference foci ratio ≥ 4) revealed by fluorescence *in situ* hybridization (FISH) in the MCF7(L/RN)-TamR

compared to P cells (**Fig. 1c** and **d**, and **Supplementary Fig. S2b** and **c**). Even in the MCF7(L/RN)-P cells, we found a mixed pattern of cell population with over 50% of cells showing > 2 fold of foci ratio, suggesting some level of *FOXA1*-CNG preexisting in the P cells even before developing endocrine resistance. Indeed, the *FOXA1* copy number (CN) in MCF7(L/RN)-P cells was higher than that in the normal mammary epithelial MCF10A cells (**Supplementary Fig. S2a**). In addition, MCF7 cells had the highest *FOXA1*-CN among a panel of 59 breast cancer cell lines (Cancer Cell Line Encyclopedia[22]) (**Supplementary Fig. S3**), perhaps due to its sub-clonal *FOXA1* amplification/CNG. These data suggest a sub-clonal selection/enrichment favoring the outgrowth of *FOXA1*-amplified cells during the development of Tam resistance in the MCF7L/RN cell lines. A relatively modest but significant *FOXA1*-CN increase was also observed in the TamR but not EDR derivatives of the BT474 model compared to P cells (**Supplementary Fig. S2a**). *FOXA1* amplification was not found in another two ER^+ Endo-R preclinical models (ZR75-1 and 600MPE).

FOXA1 is overexpressed in Endo-R derivatives and is essential for both P and Endo-R cell growth in multiple preclinical cell models. Although *FOXA1* amplification/CNG was seen mostly in MCF7(L/RN) and BT474 TamR derivatives, FOXA1 mRNA levels were higher in the TamR derivatives of all 4 preclinical models [MCF7(L/RN), BT474, ZR75-1, and 600MPE] measured by quantitative reverse-transcription (qRT)-PCR (**Fig. 2a**). Similarly, increased level of FOXA1 mRNA was also observed in the EDR derivatives of ZR75-1, 600MPE, and BT474 models. Increased FOXA1 protein levels measured by Western blotting were observed in the Endo-R derivatives compared to their P cells in some of the models (**Fig. 2b**). Importantly, FOXA1 overexpression was also observed in our previously archived *in vivo* MCF7L acquired Endo-R (TamR and EDR) xenograft tumours compared to oestrogen-treated control by immunohistochemistry (IHC) (**Fig. 2c**). ER protein was retained in most of the cell models with an increased expression in some Endo-R derivatives compared to P cells; whereas, the ZR75-1 Endo-R model had no detectable ER. Protein levels of classical ER-regulated genes like *PR* and *BCL2*, as well as *GATA3*, which is also regulated for ER transcriptional expression, were down-regulated in most of these Endo-R derivatives compared to P cells (**Fig. 2b** and **Supplementary Fig. S4**), suggesting a continuous blockade of classical ER transcriptional program.

To determine the role of ER and FOXA1 in endocrine resistance, we evaluated the cell growth of various P and their resistant derivatives of various preclinical models in response to two verified siRNAs targeting ER and FOXA1 (**Fig. 2d** and **Supplementary Fig. S5**). Knocking down ER in the MCF7(L/RN) models significantly inhibited both P and Endo-R cell growth (**Fig. 2e** and **f**). Both ZR75-1-P and 600MPE-P cells were also sensitive to ER knockdown; however, cell growth was affected to a lesser extent by ER knockdown in their Endo-R derivatives (**Fig. 2g** and **h**). On the other hand, FOXA1 knockdown substantially inhibited the growth of P and Endo-R derivatives of all the preclinical models, suggesting an important role of FOXA1 on breast cancer cell growth even in the setting of endocrine resistance.

FOXA1 overexpression-dependent gene signature is associated with and contributes to endocrine resistance. To better understand the role of increased FOXA1 in Endo-R cells, we established a stable MCF7L/FOXA1 cell model with doxycycline (Dox)-inducible FOXA1 overexpression. The extent of FOXA1 overexpression in the MCF7L/FOXA1 cells after Dox induction *vs*. without Dox was comparable to that observed in the MCF7L-TamR *vs*. P cells (**Fig. 3a**). RNA-Seq analysis revealed a total of 440 genes up-regulated and 217 genes down-regulated ($|Gfold|^{23} > 1.5$) in +Dox *vs*. -Dox cells (**Fig. 3b**). Functional annotation of these up-regulated genes in DAVID[24] showed a robust enrichment of Gene Ontology (GO) terms that included cell motion and migration, response to hypoxia, and blood vessel development ($P < 0.001$). Interestingly, within the down-regulated genes, the most enriched GO term were response to oestrogen ($P = 0.0015$), suggesting a reduction of ligand-dependent classic ER transcriptional activity in this model, which could be partly due to the decreasing level of ER itself (**Fig. 3b**, lower panel). We further used the Gene Set Enrichment Analysis (GSEA)[25] to interrogate the oncogenic gene signatures from MSigDB[26]. The MCF7L/FOXA1 gene expression profile was highly correlated to the gene sets enriched in MCF7 cells overexpressing ligand-activated EGFR or constitutively active MEK1, or in epithelial cell lines overexpressing an oncogenic KRAS (**Supplementary Table S1**, $P < 0.01$, FDR < 0.05), suggesting the enhancement of GFR and downstream signaling induced by FOXA1 overexpression. In addition, this FOXA1-induced transcriptomic profile was significantly enriched for the gene sets that were up-regulated in the MCF7 xenograft tumours resistant to multiple endocrine therapy and specifically to Tam from our previously published studies[4, 5] (**Fig. 3c**

and **d**). These data suggest that increased FOXA1 potentially drives a transcriptional program associated with high GFR signaling that contributes to tumour aggressiveness and endocrine resistance.

Since the specific gene expression of our FOXA1-overexpressing preclinical cell model resembled that of endocrine resistance, we asked whether the relationship of FOXA1 levels with endocrine resistance is also reflected in the intrinsic gene expression profiles from clinical samples. Indeed, mRNA levels of FOXA1 in a total of 752 ER+ tumours[27] were positively correlated to the two Endo-R gene signatures (**Fig. 3e** and **f**, Pearson correlation, $P < 0.001$). Next, we tested the endocrine response in our Dox-induced FOXA1-overexpressing MCF7L and ZR75-1 cell models. Increased FOXA1 expression significantly decreased the endocrine sensitivity in a FOXA1 level-dependent manner in both models (**Fig. 3g** and **h**). This stoichiometric role of FOXA1 in treatment response was also reflected in clinical samples. In a meta-analysis of ER^+ tumours[28], we found that the top-quartile of FOXA1 mRNA levels predicted poor relapse-free survival (RFS) in patients receiving Tam ($n = 615$, $P = 0.029$), but not in patients without endocrine therapy ($n = 500$, $P = 0.81$) (**Supplementary Fig. S6a** and **b**). Furthermore, the top-quartile FOXA1 overexpression predicted poor distant metastasis-free survival (DMFS) in patients with ER^+ tumours receiving endocrine but no chemotherapy ($n = 481$, $P = 0.032$) (**Supplementary Fig. S6c)**. Collectively, these data suggest that high FOXA1 expression is functionally, biologically, and clinically associated with endocrine resistance.

***FOXA1* CNG-associated gene signature predicts poor outcome in patients with ER^+ tumours.** Amplification of the genomic region encompassing the *FOXA1* gene has been reported in primary or metastatic tumours of esophagus, lung, thyroid, and prostate[29-34]. However, a molecular subtype-specific analysis of *FOXA1* CNG has not been reported in breast cancer. Analysis of the Cancer Genome Atlas (TCGA)[35] dataset revealed that *FOXA1*-CN was higher in both luminal and HER2 subtypes than in the basal subtype (**Fig. 4a**), which coincided with the FOXA1 mRNA levels (**Supplementary Fig. S7**). Within the luminal subtype of breast cancer, *FOXA1*-CN was higher in the more aggressive luminal B than in the luminal A subtype. Interestingly, using a public Gene Expression Omnibus (GEO) dataset[36], we found that *FOXA1*-CN was elevated in most matched lymph-node metastases compared to their primary ER^+ luminal tumours ($n = 22$) (**Supplementary Fig. S8**, $P = 0.0002$). To gain more clinical insight, we used the available RNA-Seq data of

583 ER^+ tumours in TCGA to identify genes that are enriched in tumours either with or without *FOXA1*-CNG ($log_2(CN/2) > 0.5$) (**Fig. 4b**). Using this *FOXA1*-CNG associated gene signature (FoCAS) (top 50 high and top 50 low genes), we queried our mega-set of breast cancer[27] with gene expression profiles and outcome data by using a *t*-score method[37]. Strikingly, the FoCAS scores significantly predicted poor disease-free survival of patients with ER^+ (n = 665), but not ER^- (n = 296) tumours (**Fig. 4c** and **d**, P = 9.69e-13 *vs.* P = 0.156). However, there was no significant difference in stratification by FoCAS between ER^+ patients treated with and without Tam (data not shown), suggesting that the FoCAS was more prognostic than therapeutically predictive in ER^+ patients. These findings suggest an unappreciated role of *FOXA1*-CNG with its associated gene expression profile in contributing to clinical outcome in ER^+ breast cancer.

Proteomic profiles perturbed by FOXA1 overexpression are associated with multiple oncogenic pathways. Because of the clinical evidence for the potential role of FOXA1 in mediating endocrine resistance, we wanted to further dissect its downstream signaling pathways. For this, we applied reverse-phase protein arrays (RPPA) to determine the proteomic changes in our FOXA1-overexpressing ER^+ cell models, using a total of 187 validated antibodies. Proteins differentially expressed between +Dox (at day 2 or 5) and -Dox samples were identified (**Supplementary Table S2**, one-way ANOVA, $P < 0.05$) and visualized in heat maps following hierarchical clustering (**Fig. 5a-c**). Consistent with the RNA-Seq data, the protein levels of ER and the products of its classical regulated genes (e.g., *PR, BCL2,* and *MYC*) were decreased in the MCF7L/FOXA1 +Dox cells (**Supplementary Fig. S9**). Assigning the total proteins assessed by RPPA into KEGG[38]-defined cancer pathways, we tracked the pathway activation status by comparing the averaged signals within each pathway between +/- Dox samples. We found that the GFR pathways of the focal adhesion, ERBB2, and insulin receptor were activated in both the MCF7L/FOXA1 +Dox and ZR75-1/FOXA1 +Dox cells (**Fig. 5d** and **e**, $P <$ 0.001). The tumour suppressor pathways (e.g., p53 and NOTCH in this analysis) were not perturbed by the FOXA1 overexpression. The decreased ER and increased GFR downstream signaling in the MCF7L/FOXA1 +Dox cells was further confirmed by Western blotting showing a FOXA1 level-dependent effect (**Supplementary Fig. S10**). Less enhanced GFR signaling were found in the 600MPE/FOXA1 +Dox cells, possibly due to an endogenously hyper-activated MAPK pathway from a *KRAS* mutation in this line[39] (**Fig. 5f**).

We also performed RPPA analysis in the MCF7L-TamR cells with FOXA1 knockdown. Interestingly, the levels of proteins related to the classical ER pathway such as PR and GATA3, which were decreased in TamR *vs.* P cells, were restored by FOXA1 knockdown (**Supplementary Fig. S11a**). Furthermore, FOXA1 knockdown in MCF7L-TamR cells suppressed the oncogenic pathways (e.g., ERBB2 and insulin receptor), which otherwise were enhanced in FOXA1-overexpressing P cells (**Supplementary Fig. S11b**). The overall proteomic changes in the P cells with FOXA1 overexpression were inversely correlated to the changes in the TamR cells with FOXA1 knockdown (Pearson's $R^2 = 0.416$). Together with previous transcriptomic data, these findings pointed to a dominant role of increased FOXA1 in strengthening oncogenic signaling pathways in endocrine resistance, with an inhibitory effect on ER expression and classical ER transcriptional activity.

An integrative approach identifies *IL8* as one of the most perturbed genes regulated by FOXA1 in Endo-R cells. To further investigate the direct impact of FOXA1 on gene expression, we performed FOXA1 genome-wide chromatin immunoprecipitation followed by high-throughput seq (ChIP-Seq) in MCF7L-P and TamR cells. A total of 37,227 and 53,215 FOXA1 binding events were found in MCF7L-P and TamR cells, respectively (**Supplementary Fig. S12**). Among these binding events, there were 21,449 shared FOXA1 binding which accounted for 58% and 40% of total binding events in P and TamR cells, respectively. Within the distinct binding events in P and TamR cells, the highest enrichment of FOXA1 motif was followed by the GATA motif in P cells, and the BCL11A and JUN/FOS motifs in TamR cells, suggesting the significant FOXA1 binding in both P and TamR cells albeit on different sites. In parallel, we also obtained the transcriptomic profiles of both MCF7L-P and TamR cells using RNA-Seq. In an effort to identify the downstream signaling associated with FOXA1 in endocrine resistance, we integrated these RNA-Seq with the FOXA1 ChIP-Seq data described above. All the genes identified in RNA-Seq were sorted by their expression ratio (TamR *vs.* P), and the number of the identified FOXA1 binding sites (tags) for each gene was counted within 20 kilobases (kb) from their transcription start sites (TSS). The genes preferentially expressed in either TamR or P cells tended to have more FOXA1 tags, supporting the notion that FOXA1 is indeed important for defining the distinct gene patterns in both TamR and P cells (**Fig. 6a**).

Next, we focused on the genes highly expressed in MCF7L-TamR compared to P cells (log_2fold > 1.5, FDR < 0.05) and that also carry the most abundant FOXA1 tags in TamR cells around their gene regions (log_{10}fold > 1.5) (**Fig. 6b**). Interestingly, the enriched GO terms within these top genes included the blood vessel development (*IL8, CTGF, LOX*, and *ROBO1*), response to wounding (*BMP2*, *CTGF*, *DCBLD2*, *IL8*, and *LOX*), and cell migration (*CTGF, IL8, NR2F1*, and *ROBO1*), reminiscent of the GO terms enriched in the FOXA1-overexpressing MCF7L-P cells. Indeed, four genes (*IL8*, *LOX*, *NR2F1*, and *CTGF*) were highly up-regulated in MCF7L/FOXA1 +Dox cells, suggesting FOXA1-dependent regulation. Furthermore, we found that there was a significant overlap between the genes highly represented in MCF7L/FOXA1 +Dox cells (n = 440, Gfold > 1.5, FDR < 0.05) and the TamR signature genes (n = 428, $|log_2fold| > 1.5$, FDR < 0.05). These genes again included *IL8* and *CTGF*, further supporting the FOXA1-depended mechanism of Tam resistance (**Fig. 6c**, Fisher's exact test, $P < 0.0001$). Importantly, we also identified 10 genes (including *IL8* and *CTGF*) within the Fig. 6b gene list that were down-regulated by ER knockdown in MCF7L-TamR cells (RNA-Seq data not shown), suggesting an ER-dependent mechanism in gene regulation by increased FOXA1.

We verified the robust increase in mRNA levels of *IL8*, the gene at the top of the list, in our two independent TamR cell models from MCF7 line (L and RN) by qRT-PCR (**Fig. 6d**). In addition, the significant increase in IL-8 expression was also found in both 600MPE and ZR75-1 Endo-R cell derivatives compared to their P cells, though the magnitude was much smaller in ZR75-1 model. Since ER expression is maintained in these Endo-R cells except the ZR75-1 model, we postulated that the robust up-regulation of IL-8 might need both ER and FOXA1. It has been reported that FOXA1 mediates differential ER-chromatin binding program in ER^+ tumours from patients with poor outcome[18]. We hypothesize that increased FOXA1 may contribute to ER transcriptional reprogramming in our Endo-R cell models. To better appreciate the impact of increased FOXA1 on transcriptional switching of ER from ligand-dependent to ligand-independent and GFR signaling-activated program, we further integrated our RNA-Seq data in MCF7L/FOXA1 cells with the existing ER/FOXA1 cistromic data in MCF7 cells[40, 41]. Searching the ER/FOXA1 binding within 20 kb near the TSS, we predicted the genes to be regulated by FOXA1, or ER stimulated by E2 or epidermal growth factor (EGF). A Venn diagram showed vast overlaps as well as distinct subsets among these cistrome-defined gene sets (**Fig. 6e**).

Next, we examined the distribution of differentially expressed genes induced by FOXA1 overexpression across these overlapping gene subsets. Specifically, FOXA1-up-regulated (UP) genes were highly enriched in the gene sets with both FOXA1 and EGF-not-E2 or EGF-and-E2-stimulated ER binding (n = 1,811 and n = 1,666, respectively) (**Fig. 6f** and **g**). Notably, *IL8* and *CTGF* were found again in the get set with both FOXA1 and EGF-not-E2-stimulated ER bindings, suggesting the regulation under FOXA1 and ER in the context of high growth factor signaling. FOXA1-down-regulated (DN) genes were only enriched in the gene set with both FOXA1 and EGF-and-E2-stimulated ER binding (**Fig. 6g**). In contrast, no enrichment of any FOXA1-altered or non-altered (NA) genes was found in the gene set with both FOXA1 and E2-not-EGF-stimulated ER binding (n = 309) (**Fig. 6h**). These data suggest that high levels of FOXA1 may coordinate with ER in transcriptional reprogramming towards a more growth factor induced-cistromic profile.

Increased FOXA1, together with ER, co-regulate IL-8 expression. Next, we aimed to investigate the regulation of IL-8 as it was the most perturbed gene identified from our integrative approach. Previous cistromic data in MCF7 cells[40, 41] revealed that there were two FOXA1 binding sites at distal region (*dis.*) and proximal region (*pro.*) upstream of the *IL8* TSS, and one EGF-stimulated ER binding site at the *dis*. (**Fig. 7a**). Our FOXA1 ChIP-Seq data showed that the FOXA1 binding to these regions in MCF7L-TamR cells was enhanced compared to that in MCF7L-P cells (**Fig. 7b**). Using ChIP followed by qPCR, we verified the enhancement of FOXA1 binding at both *dis.* and *pro*. in MCF7L-TamR cells (**Fig. 7c**). Furthermore, there was an enhanced recruitment of ER at the *dis.* in MCF7L-TamR cells, the same region where ER bound in EGF-treated MCF7 cells, suggesting that ER regulates IL-8 in a ligand-independent manner in TamR cells. IL-8 levels in the two TamR cell models (MCF7L and 600MPE) were reduced by either ER or FOXA1 knockdown (**Fig. 7d** and **e**), with the strongest reduction in the MCF7L-TamR cells from knockdown of FOXA1, suggesting that these binding events are also biologically relevant. In parallel, IL-8 expression was dramatically induced by FOXA1 overexpression in MCF7L-P cells; the increasing IL-8 by FOXA1 was substantiously reduced by simultaneous ER knockdown (**Fig. 7f**). This phenomenon could be recapitulated in a second 600MPE/FOXA1 cell model (**Fig. 7g**), supporting the notion that high levels of FOXA1 and ER might co-regulate IL-8 expression. In line with the increased FOXA1 and ER protein levels in our MCF7L Endo-R xenograft tumours

(**Fig. 2c** and **supplementary Fig. S13**), IL-8 expression was also up-regulated in both TamR and EDR tumours in this xenograft model (**Fig. 7h** and **i**). Moreover, we measured FOXA1 and IL-8 expression in a total of 85 ER^+ human primary breast tumours integrated in a tissue microarray. FOXA1 staining was prevalently localized in the nuclei; while IL-8 staining was mainly in paranuclear region of cancer cells in 54% of these tumours (**Fig. 7j**). The same paranuclear staining of IL-8 was also seen in both MCF7L-TamR xenograft tumours (**Fig. 7h**) and *in vitro* TamR cells (**Supplementary Fig. S14**). Importantly, the proportion of IL-8 positive tumours gradually increased with increasing FOXA1 in the 85 ER^+ human primary breast tumours (**Fig. 7k**), indicating a stoichiometric role of FOXA1 in regulating IL-8.

IL-8 mediates the effect of augmented FOXA1 on cell growth, invasion, and endocrine resistance. To evaluate the role of IL-8 as a downstream effector of increased FOXA1 in endocrine resistance, we obtained the transcriptomic profiles of MCF7L-TamR cells with FOXA1 or IL-8 knockdown by using RNA-Seq. Interestingly, comparing to the genes differentially expressed in TamR cells upon FOXA1 knockdown ($|Gfold| > 0.5$), there was a striking similarity in the expression patterns of these same genes in TamR cells upon IL-8 knockdown (**Supplementary Fig. S15**), indicating a crucial role of IL-8 in the gene expression perturbations induced by FOXA1 in Endo-R cells. Similar to FOXA1 knockdown, IL-8 knockdown potently inhibited cell growth in both MCF7L-P and TamR cells, with a more growth inhibitory effect in TamR than P cells (**Fig. 8a**). This knockdown effect could be rescued by co-expression of an IL-8 cDNA with the IL-8 siRNA sequences (#2) targeting the 3'-UTR region of *IL8* gene, but not with the other siRNA (#1) targeting the coding region of *IL-8* (**Supplementary Fig. S16**). However, this IL-8 knockdown-induced cell growth inhibition was not seen in 600MPE-P and TamR cells (**Fig. 8b**). Since FOXA1 knockdown in MCF7L-TamR cells suppressed multiple oncogenic pathways that otherwise were upregulated in FOXA1-overexperssing P cells (Supplementary Fig. S10 and S11), we asked whether IL-8 knockdown in TamR cells leads to a similar change in signaling. Indeed, the activated signaling of multiple GFR downstream pathways (e.g., pAKT, pMAPK, and pS6) in TamR cells was reduced by IL-8 knockdown (**Fig. 8c**). To further investigate the relationship of IL-8 and FOXA1 in endocrine response, we established a series of inducible MCF7L cell lines with overexpression of YFP (control) or FOXA1 combined with concomitant knockdown of luciferase (Luc, control) or IL-8 upon induction by Dox.

As a result, the increased IL-8 upon FOXA1 induction was substantially reduced by co-expression of IL8-shRNA (**Fig. 8d**). In contrast, FOXA1 induction was not interfered by IL8 knockdown. Without Dox, all the MCF7L stable lines showed similar sensitivity to endocrine treatment (**Supplementary Fig. S17**). With Dox, IL-8 knockdown alone or FOXA1 overexpression alone partially increased or decreased the endocrine sensitivity, respectively (**Fig. 8e**). Importantly, the reduced endocrine sensitivity by overexpressing FOXA1 could be partially recovered by concomitant IL-8 knockdown, suggesting that IL-8 indeed is one of the key downstream mediators of FOXA1 in conferring endocrine resistance. Finally, we applied RPPA to measure the signaling changes upon concomitant FOXA1 overexpression and IL-8 knockdown. Again, the enhanced signaling in multiple GFR downstream pathways after FOXA1 overexpression was suppressed by IL-8 knockdown (**Fig. 8f**), suggesting that the contribution of IL-8 to FOXA1-induced endocrine resistance is partially through mediating the GFR downstream signaling enhanced by high FOXA1 expression.

Since deregulated IL-8 signaling also contributes to cancer cell migration, invasion, and metastasis[42-44], we next evaluated the role of IL-8 in cell invasiveness. We found that IL-8 knockdown significantly diminished cell invasion in MCF7L-TamR cells, which were more invasive than MCF7L-P cells where IL-8 knockdown did not have a significant effect (**Fig. 8g**). Both 600MPE-P and TamR cells showed stronger invasiveness, possibly due to the constitutively activated RAS/RAF/MAPK pathway. IL-8 knockdown partially mitigated the invasiveness of both 600MPE-P and TamR cells (**Fig. 8h**). In parallel, FOXA1 overexpression in both MCF7L-P and 600MPE-P cells enhanced cell invasion, which was abrogated by IL-8 knockdown (**Fig. 8i** and **j**). These findings support a role of IL-8 in mediating cell invasion in both TamR and FOXA1-overexpressing P cells.

Discussion

In an effort to characterize our breast cancer Endo-R cell models, we discovered for the first time a gene amplification of the ER pioneer factor FOXA1 in two independent TamR derivatives from MCF7 line. A recent clinical study using next-generation sequencing also identified *FOXA1* gene amplification in 1 out of 20 cases of ER^+ residual disease after 6-month neoadjuvant endocrine therapy[45]. Recent studies unveiled gain-of-function mutations in *ESR1*, the gene encoding ER, in 15-20% of metastatic ER^+ Endo-R tumours[46-49]. Therefore, genomic amplification or overexpression of FOXA1 may be another mechanism for endocrine

resistance in advanced ER^+ disease. We found *FOXA1*-CNG in 14% of the TCGA luminal tumours, which give rise to a gene signature of FoCAS that robustly predicts poor outcome only in ER^+ patients. It is plausible that a process of sub-clonal selection might favor the outgrowth of the rare population with *FOXA1* amplification/CNG within primary tumours for developing endocrine resistance and late recurrence. To test this hypothesis, we expect that the CN analysis (e.g., FISH) of *FOXA1* in ER^+ metastases or residual disease after endocrine therapy would uncover *FOXA1* gene aberrations associated with disease progression and endocrine resistance.

In addition to gene amplification, increased FOXA1 expression occurs at either mRNA or protein level in our Endo-R cell models. We showed that overexpressing FOXA1 in ER^+ breast cancer cells vigorously activated multiple oncogenic pathways at both transcriptomic and proteomic levels, leading to endocrine resistance and enhanced cell invasion. Moreover, knockdown of FOXA1 in TamR cells suppressed the corresponding oncogenic/GFR downstream signaling, leading to the decreased cell growth in all our tested Endo-R cell models. High levels of FOXA1 in prostate cancer have been shown to increase the growth of cancer cells and xenograft tumors, and correlate with poor prognosis[30, 50]. In contrast, high levels of FOXA1 in breast cancer have generally been regarded as a marker of good prognosis[16]. As a luminal lineage marker, FOXA1 promotes the differentiation of normal mammary epithelial cells; and in cancer cells may engage in a more differentiated transcriptional program of hormone receptors like ER. Therefore, it is possible that FOXA1 expression in ER^+ tumours indicates a classical ER transcriptional program that can be effectively targeted by anti-oestrogen therapy. Previous studies from us and others have shown that during the ER^+ disease progression, ER switches from a ligand-dependent to ligand-independent and GFR signaling-stimulated transcriptional program, leading to endocrine resistance[3-5, 18, 41]. We report here that increase in FOXA1 coordinates with ER in this reprogramming, leading to perturbed gene signatures and signaling pathways associated with endocrine resistance. As such, our data support the role of FOXA1 overexpression in more aggressive tumours, which is in line with the findings of high levels of FOXA1 in both breast and prostate cancer metastases[18, 51]. Moreover, using *in silico* data, we showed that the perturbed genes in FOXA1-overexpressing MCF7L-P cells, tend to enrich for both FOXA1 and EGF-stimulated ER binding, which

conforms to a study in MCF7 cells showing a rapid reprogramming of ER binding mediated by FOXA1 in response to a combination of mitogens[18]. Therefore, increased FOXA1 may also drive ER transcriptional reprogramming and endocrine resistance. Strong evidence also comes from prostate cancer where increased FOXA1 in androgen-responsive prostate cancer cells facilitates AR-chromatin binding at novel regions and promotes castration-resistant and androgen-independent cell growth[52].

How exactly does increased FOXA1 induce endocrine resistance? Through an integrated cistromic and transcriptomic approach, we identified IL-8 among the most perturbed genes regulated by FOXA1 in TamR cells. IL-8 was regulated by both FOXA1 and ER; however, not all genes from our integrated analysis were regulated by ER, suggesting an ER-independent mechanism of FOXA1 in endocrine resistance. Substantial evidence indicates that increased IL-8 levels promote tumour-initiating cell survival, tumour invasion, metastases[42], and therapy resistance[43, 53]. However, in ER^+ breast cancer, the role of IL-8 and its mediated inflammation remains to be determined. It has been reported that an inflammatory gene signature identified in ER^+ breast tumours was associated with poor response to aromatase inhibitor[54]. We found that IL-8 mediated the effect of increased FOXA1 on cell growth and invasion in our Endo-R cell models. It is intriguing to extrapolate the findings of IL-8 from our cell models, where mainly involves an autonomous role, to *in vivo* tumours with stromal contents that conferring paracrine effect. Notably, our preliminary data (unpublished) suggested a possible intracellular IL-8 signaling in endocrine resistance, a mechanism proposed before in prostate cancer[55]. IL-8 knockdown effectively inhibited cell growth and invasion, especially for TamR cells, supporting the development of a new approach to treat Endo-R tumours by targeting IL-8.

Collectively, we report a novel gene amplification in *FOXA1* in Endo-R cell models. Sub-clonal evolution and FOXA1/ER transcriptional reprogramming may co-exist as the underlying mechanism of endocrine resistance. IL-8 signaling is one of the components embedded in the FOXA1/ER transcriptional reprogramming, and provides a potential therapeutic target for ER^+ tumours with increased FOXA1.

Methods

Cell culture. The Endo-R derivatives were developed from P cells of MCF7L (M. Lippman), 600MPE (J. Gray), ZR75-1 (American Type Culture Collection), and BT474 (AstraZeneca), using the method as we

previously reported[56]. The MCF7RN Endo-R cell model was kindly provided by R. Nicholson (Cardiff, UK). All the cells were authenticated and the P cells were maintained in RPMI/1640 (MCF7, ZR75-1) or DMEM/high-glucose (600MPE, BT474), supplemented with 10% heat-inactivated fetal bovine serum (FBS) and 1% penicillin/streptomycin/glutamine (PSG). The Endo-R cells were kept in phenol-red free (PRF) medium supplemented with 10% heat-inactivated charcoal-stripped (CS)-FBS and 1% PSG, with (TamR) or without (EDR) the addition of 100 nM 4-OH-tamoxifen (H7904, Sigma). The Dox-inducible FOXA1 overexpressing cell lines were established using a lentiviral cDNA delivery system (from X. Pan, Novartis, USA), and maintained by 200 μg ml^{-1} Geneticin (Invitrogen). The Dox-inducible shIL-8 knockdown cell lines were established using the pINDUCER system[57]. All cells were incubated at 37°C in 5% CO_2.

Exome-Seq and CNG analysis. Whole-exome-seq was performed using the DNA samples from MCF7(L/RN)-P and TamR cells. (Laura: Please describe the Exome-seq method and CN data analysis.) … *FOXA1*-CN data from the TCGA ER^+ tumours was also acquired from the GISTIC analyzed data of Affymetrix 6.0 SNP arrays[35]. *FOXA1*-CNG was defined as $\log_2(CN/2) > 0.5$. The differentially expressed genes between the tumours with and without *FOXA1*-CNG were identified by using the ComparativeMarkerSelection module from the GenePattern[58] with a FDR < 0.05. The top50 enriched genes with opposite directionalities (a total of 100) were used for further analysis.

FISH. Four-micron thick formalin-fixed and paraffin-embedded (FFPE) cell pellet sections were baked at 56°C, dehydrated, and air-dried before pretreatment. In an effort to increase the intensity of the hybridization signals, we chose two BAC clones (RP11-356O9 and CTD-2386P23) to cover the *FOXA1* gene at chromosome 14q21.1, and additional two BAC clones (RP11-314P15 and CTD-2595D15) to target a non-relevant reference region (*REF*) at chromosome 14q12. BAC clones RP11-314P15 and RP11-356O9 were obtained from the BAC-PAC Resource at Children's Hospital Oakland Research Institute. BAC clones CTD-2595D15 and CTD-2386P23 were obtained from Life Technologies. A nick translation kit (Abbott Molecular) was used to make the *FOXA1* and *REF* probes labeled with Spectrum Green and Red dUTPs, respectively. The labeled probes were air-dried, followed by reconstitution in nuclease-free water and **hybridization buffer** (Abbott Molecular). After denaturation, hybridization was performed at 37°C for 16 h in a Thermo Hybrite (Abbott Molecular).

Hybridized slides were then washed in 2 × SSC buffer with 0.3% IGEPAL (Sigma) once at 70°C for 2 min, and twice at room temperature (RT) for 1 min. Slides were counter-stained in Vectashield mounting media with DAPI (Vector Laboratories) and then imaged using an Olympus BX51 microscope. Individual images were captured using a Leica Imaging system running CytoVision (v7.4). A minimum of 50 individual cell nuclei were scored per specimen. Nuclei were scored as containing 1, 2, 3, 4, or >4 signals for both red (*REF*) and green (*FOXA1*). A *FOXA1* to *REF* ratio (F:R) was then generated by averaging the obtained ratios. Specimens with an overall F:R ratio between 0.8 and 1.1 were considered as having no *FOXA1* CN changes, ratio between 1.2 and 2.5 as having *FOXA1* CNG, and ratio of 4 or higher as having *FOXA1* amplification.

gPCR assay. DNA was extracted from asynchronous cells using the Wizard Genomic DNA Purification Kit (Promega). *FOXA1*-CN was measured using the qBiomarker Copy Number PCR assay (Qiagen). Briefly, in parallel to *FOXA1* PCR assay, a Multicopy Reference Copy Number PCR assay (Mref) was applied to provide normalization for DNA input. Real-time PCR was used to determine the CN status of a particular sample using the $\Delta\Delta C_T$ method by comparing the test sample (cancer cells) with a reference genome (MCF10A, diploid cell control).

Western blotting. This assay was performed as described previously[59]. Primary antibodies used in this study are: ER (ab9269) and FOXA1 (ab23738) from Abcam; PR (sc-7208) from Santa Cruz Biotechnology; phosphorylated (p) STAT3-S727 (cs9134), pAKT-S473 (cs9271), pMAPK-T202/Y204 (cs9101), pS6-S235/236 (cs2211), and β-actin (cs4970) from Cell Signaling Technology. All Western blots shown are from the same gel with the same exposure.

Animal Studies. Animal care and animal experiments were in accordance with and approved by the Baylor College of Medicine Institutional Animal Care and Use Committee (IACUC). We used the archived formalin-fixed and paraffin-embedded xenograft tumours of MCF7L Endo-R *in vivo* model derived from our previously published study[56].

RNA interference. Cells were transfected with si-FOXA1_ #1 (HSS104880) or #2 (HSS179280) (Invitrogen), or si-ER_#1 (VHS40912) or #2 (VHS40913) (Invitrogen), or si-IL8_#1 (SI02654827) or _#2 (SI02654834) (Qiagen). The siRNA SMART Pool (ON-TARGET plus, Dharmacon) was used to knockdown CXCR1 or

CXCR2. The siRNA controls are the siRNA against Luciferase (Invitrogen), the AllStars Negative Control siRNA (Qiagen), or the ON-TARGET plus Non-targeting Pool (Dharmacon) with no homology to any known mammalian gene. Transfection was performed using RNAiMAX (Invitrogen) according to the manufacturer's instructions. Cell lysates were collected at 72 h after transfection for Western blotting. Transfection efficiency was comparable between MCF7L-P and TamR, as shown by the protein reduction in Western blots.

Cell growth assay. Cells were pre-treated in PRF medium with 5% CS-FBS and -/+ Dox for 48 h and then split and grown in a 96-well plate with 2,000 cells well^{-1} for an additional 48 h before treatment. Culture media with drugs were replaced every three days for a total of 4~6 days. Cell numbers were quantified by colorimetric methylene blue staining[59]. Cell growth under E2 was set as the normalization control. All the anti-oestrogen treatments (ED, Tam, and Ful) were in the absence of E2. The relative cell growth was determined by (OD at day$_n$ - OD at day$_0$) $_{\text{Treatment}}$ / (OD at day$_n$ - OD at day$_0$) $_{\text{E2}}$ × 100%.

RNA-Seq and gene expression analysis. RNA samples from the MCF7L-P and MCF7L-TamR cells were isolated using… (Laura: Please describe the methods for RNA extraction, library preparation, sequencing platform, and data processing). The RNA samples from the MCF7L-P/FOXA1±Dox cells, MCF7L-TamR cells with siRNA knockdown of N.S., FOXA1, and IL-8, were isolated using … (Rinath: Please describe the methods for RNA extraction, library preparation, sequencing platform, and data processing). Differential expression analysis was performed using the Gfold method[23], and the genes with an absolute Gfold value > 1.5 were presented in a heat map using Java Treeview[60]. Functional annotation of the differentially expressed genes upon FOXA1 overexpression was performed using GO Term analysis in DAVID[24]. GSEA was performed for pathway analysis of differentially expressed genes using the Molecular Signatures Database (MSigDB, v5.0)[26]. Fisher's exact test was used to assess the correlation of two gene sets with overlapping genes. All the RNA-Seq data have been deposited in the Gene Expression Omnibus database under GSE…(Should we submit all RNA-seq data here and the FOXA1 ChIP-seq data together and acquire one GSE number?)

Kaplan-Meier Curves. Tumours from a mega-set of breast cancer[27] with available gene expression profiles and outcomes were stratified to top-, medium-, and low-FoCAS score groups using a signature *t*-score

method[37]. Disease-free survival (DFS) was analyzed separately for ER^+ and ER^- patients among these tertiled groups using the log-rank survival test.

RPPA and signaling pathway analysis. RPPA was performed in the Baylor College of Medicine Proteomics Core Facility. Lysates were extracted from 3 biological replicates of each cell sample using RPPA lysis buffer (1% Triton X-100, 50 mM HEPES, pH 7.4, 150 mM NaCl, 1.5 mM $MgCl_2$, 1 mM EGTA, 100 mM NaF, 10 mM Na-pyrophosphate, 1 mM Na_3VO_4, 10% glycerol, containing freshly added protease and phosphatase inhibitors (Roche)). The supernatant after centrifugation was quantitated using the BCA Assay Kit (Thermo Scientific). Proteins with concentrations adjusted to 1.5 $\mu g\ \mu l^{-1}$ by diluting in 1% SDS loading buffer (with beta-mercaptoethanol) were denatured and spotted on the RPPA with 3 replicates. The signal for each spot was subtracted by the corresponding negative control signal for that spot and followed by total protein normalization. Differentially expressed proteins across samples were determined by one-way ANOVA and the expression values were log_2-transformed and mean-centralized for visualization in heat maps using Java Treeview. Proteins were categorized according to the KEGG-defined pathways and each group of proteins belonging to the same pathway was compared between samples of interest, by using the paired one-sided *t*-test. The concordance of changes in all tested pathways between the two cell lines (MCF7L-P/FOXA1 and MCF7L-TamR/siRNA) was further analyzed using the Pearson correlation test.

Integrated ChIP-seq and RNA-seq data analysis. FOXA1ChIP experiments were conducted as described previously using rabbit polyclonal anti-FOXA1 antibody (). Briefly, (Rinath: Please describe the ChIP-Seq method, data processing, motif analysis, and the integration process with RNA-Seq data). Beads were thoroughly washed and reverse-crosslinked at 65°C before amplification using the TruSeq kit (Illumina). Single-end 36-bp ChIP-seq data were generated by the Illumina analysis pipeline v1.6.1 (Illumina), and reads were aligned to the Human Reference Genome (assembly hg19, GRCh37, February 2009) using bwa 0.5.9. … Motif enrichment analysis was performed using… For the integration with RNA-seq data, we calculated the average normalized FOXA1 binding sites (tags) every 300 genes (20 kb away from their TSS), along the genes sorted from the highest to the lowest expression ratio (TamR *vs.* P) according to the RNA-seq data. Genes that

highly expressed in TamR *vs*. P cells with $\log_2$(fold) > 1.5 (FDR < 0.05) were selected and overlapped with the genes carrying highly enriched FOXA1 tags in TamR *vs*. P cells with $\log_{10}$(fold) > 1.5.

qRT-PCR. The assay procedure was described previously[61]. SYBR dye (Life Technologies) was used in real-time PCR and the target primer sequences are as follows: *ESR1* forward GGGAAGTATGGCTATGGAATCTG, reverse TGGCTGGACACATATAGTCGTT; *FOXA1* forward GCAATACTCGCCTTACGGCT, reverse TACACACCTTGGTAGTACGCC; *IL8* forward ACTGAGAGTGATTGAGAGTGGAC, reverse AACCCTCTGCACCCAGTTTTC; *GAPDH* forward AAGGTGAAGGTCGGAGTC, reverse GGGGTCATTGATGGCAAC.

Integrative cistromes analysis. Every RefSeq gene (assembly hg18, NCBI v36.1) was searched for the nearest ChIP regions upstream and downstream of transcription start sites (TSS) using the *Cis*-Elements Annotation Systems (CEAS)[62]. EGF- or E2-stimulated ER ChIP-on-chip[41] and FOXA1 ChIP-seq data[40] from MCF7 cells (peak calls at FDR < 0.2) were used to identify the cistromes-defined genes with ER or FOXA1 binding sites within ± 20 kb from the TSS. For the correlation analysis between differential gene expression and transcription factor binding, we calculated the percentage of FOXA1-overexpression regulated genes and the percentage of non-altered genes with binding sites of FOXA1 and ER (EGF-not-E2-stimulated, EGF-and-E2-stimulated, and E2-not-EGF-stimulated) in the indicated combinations within ± 20 kb from the TSS. Fisher's exact test was used to assess the statistical significance in the correlation analysis.

ChIP-qPCR. ChIP assay was performed using the Zymo-Spin ChIP kit (Zymo Research) following the manufacturer's protocol. The antibodies used for ChIP assay were anti-FOXA1 (ab23738) from Abcam, and anti-ER (sc-543) and normal rabbit IgG (sc-2027) from Santa Cruz Biotechnology. The occupancy of FOXA1 and ER on the *IL8* gene locus was analyzed by real-time qPCR using SYBR Green master mixes (Life Technologies) with the following primers: *dis.* forward AAGCCCTGGACAAATATACT, reverse CTATTCAATGACATCTGTGGTT; *pro.* forward ATAAGTTCTCTAGTAGGGTGATGA, reverse TGCTCTGCTGTCTCTGAA. The amount of specific DNA fragments from ChIP was presented as the percentage of sheared chromatin input.

ELISA. Secreted IL-8 protein was measured by a human IL-8 ELISA kit (Thermo Scientific). Briefly, samples collected from three day culture media of cells with -/+Dox and/or siRNA knockdown were diluted and added to a 96-well microtiter plate, which was coated with anti-IL-8 antibody. After 1 h incubation, the wells were washed three times and incubated with biotinylated anti-IL-8 antibody for an additional 1 h. The plate was washed three times and incubated with streptavidin-HRP conjugate for 30 min before chromogen substrate was added. The absorbance at A_{450} minus A_{550} was measured by using a microplate reader (Bio-Rad). The concentration of IL-8 was calculated from the standard curve and normalized to the protein concentration of the same sample.

IHC. This assay was performed as described previously[59]. Briefly, freshly cut 3-micron sections from paraffin-embedded blocks with integrated human breast tumours (3-mm core tissue, × 50) or cell pellets were deparaffinized and subjected to epitope retrieval in boiling citrate buffer (pH 6.0) for 20 min. After blocking in 3% hydrogen peroxide for 5 min, slides were incubated with antibody [normal IgG control (Santa Cruz Biotechnology), FOXA1 (1:200; ab23738, Abcam), IL-8 (1:500; Serotec, UK), or CXCR1 (1:100; Life Technologies)] at RT for one hour. Immunodetection was performed with the EnVision+ System (DakoCytomation). The completed slides were independently reviewed by two pathologists. The nuclear FOXA1 and paranuclear IL-8 staining was assessed using an Allred scoring system[63]. IL-8 positive tumours were defined by Allred score > 0 for correlation analysis with FOXA1 staining.

Cell invasion assay. This assay was performed in a 24-well BD Falcon™ Multiwell Insert System containing an 8-micron pore size membrane. The surface of the upper chamber was coated with 4 µg of basement membrane matrix Matrigel (BD) diluted in 50 µl of DMEM:F12 medium and allowed to air-dry overnight. The Matrigel was then re-hydrated with medium for 2 h. Cells were pre-treated -/+ Dox for 48 h before pre-starvation in serum-free medium for 24 h, and then added to upper chamber (1×10^5 cells $well^{-1}$). The lower chamber was filled with 300 µl of medium supplemented with 20% FBS and 300 µl of conditioned medium (0.45 µm filtered) obtained from cells with -/+ Dox. After 72 h of incubation, cells on the upper surface of the membrane were removed by wiping with a cotton swab, and the cells remaining on the down-side of the

membrane were fixed by 5% glutaraldehyde and stained with 1% crystal violet solution. Cell invasion was assessed by counting the cells from at least nine different fields per well under a microscope.

Statistical analysis. Statistical analysis of *in vitro* assays was based on at least triplicated data using R software (v2.13.0) or GraphPad Prism (v5.04). All experiments were repeated at least three times. Quantitative data from a representative experiment are shown as mean ± SEM. Significant difference ($P < 0.05$) was determined by ANOVA or Bonferroni post-hoc tests (multiple testing corrected), or specified above.

Acknowledgements

We thank M. Lupien for sharing ER cistromic data, S. Mao and Z. Guo for IHC, M. Trivedi and G. Chamness for reading and reviewing this manuscript. This work was supported by funds from a Department of Defense Breakthrough Award to X.F. (W81XWH-14-1-0326), a grant from the Breast Cancer Research Foundation to R.S. and C.K.O., a Stand Up to Cancer Translational Grant to R.S., C.K.O., and J.W.G (SU2C-AACR-DT0409), a National Institutes of Health (NIH) Breast Cancer Specialized Programs of Research Excellence (SPORE) Grant to C.K.O., a Dan L. Duncan Cancer Center Grant from NIH to C.K.O. (P30C125123), and Susan G. Komen for the Cure Foundation Promise Grants to C.K.O. (PG12221410) and J.W.G. (SAC110012). This work was supported in part by Cancer Prevention & Research Institute of Texas Proteomics & Metabolomics Core Facility Support Award (RP120092) and NCI Cancer Center Support Grant to Antibody-based Proteomics Core/Shared Resource (P30CA125123) at Baylor College of Medicine and the technical assistance of F. Jia, M.G. Costello, and K. Holloway. This work was also supported by the Cytometry and Cell Sorting Core at Baylor College of Medicine with funding from the NIH (P30AI036211, P30CA125123, and S10RR024574) and the expert assistance of Joel M. Sederstrom.

Author contributions

X.F., R.S., and C.K.O. designed the research. X.F. and R.P. conducted the experiments with assistance from E.F.H. and D.L.T. in FISH assay, M.S., A.N., and C.D.A. in developing Endo-R cell models. R.J. and F.L. conducted the RNA-seq and ChIP-seq with assist from M.B. L.M.H., P.A., N.W., and C.G. conducted the exome-seq and data analysis with assistance from P.S. and J.W.G. X.F., C.J.C., and A.T. performed the bioinformatics and biostatistical analysis with advice from S.G.H. S.H. and D.P.E. performed the RPPA

experiment and data processing. M.F.R. and C.G. contributed to the clinical sample collection and histological analysis. X.F. and R.S. wrote the manuscript with assistance from the other authors.

Additional information

Accession codes: The sequencing data have been deposited with the GEO under accession number GSE…

Figure legends

Figure 1 | *FOXA1* gene amplification in preclinical ER$^+$ Endo-R cell models. (**a** and **b**) Plots of whole-exome-seq data show the losses and gains of DNA sequences along the length of chromosomes 1 through X as determined by segmentation analysis of normalized CN-log2 ratios in MCF7L/RN-TamR *vs.* P cells. The arrows point to the highest focal amplification region, which includes *FOXA1*, at chromosome 14. (**c**) Representative images of bright-field and the *FOXA1*-FISH of MCF7L-P and TamR cells, show the enrichment of gene amplification in MCF7L-TamR *vs.* P cells. Green and red signals indicate the locations where *FOXA1* and chromosome 14 centromere reference (*REF*) probes were hybridized, respectively. Scale bar, 100 μm (bright field) and 20 μm (FISH). (**d**) Stacked bar chart summarizes the percentage of cells (n = 65) with *FOXA1*/*REF* foci ratio within indicated ranges. See the supplementary methods for data interpretation.

Figure 2 | Increased FOXA1 expression in multiple Endo-R cell models. (**a**) FOXA1 mRNA levels determined by qRT-PCR across all Endo-R cell models. The amount of mRNA from MCF7L-P cells was set as normalization control (= 1). (**b**) FOXA1, ER, and PR proteins recognized by Western blots using indicated antibodies across all Endo-R cell models. GAPDH was used as a loading control. (**c**) Scatter dot plots of FOXA1 Allred score in MCF7L Endo-R xenograft tumours measured by immunohistochemistry. Xenograft tumours in ovariectomized nude mice with oestrogen pellets (E2), or without E2 but treated with Tam or without Tam (ED), were harvested when the tumour volume reached 1000 mm^3. Error bars, SEM (n > 5 in each group). ***P < 0.001, Bonferroni post-hoc test (multiple testing-corrected). (**d**) Western blots show the protein levels of FOXA1 and ER in MCF7L-TamR cells with gene knockdown. (**e-h**) Cell growth within a 6-day period after siRNA knockdown of non-specific (N.S.), ER, or FOXA1 in MCF7L, MCF7RN, ZR75-1, and 600MPE Endo-R cell models. Cell growth in N.S. knockdown was used as normalization control (100%). Data

represent means ± SEM. *P < 0.05, **P < 0.01, ***P < 0.001, two-sided t-test for all comparisons between N.S. and ER/FOXA1 knockdown.

Figure 3 | FOXA1 overexpression elicits a gene signature associated with endocrine resistance. (**a**) FOXA1 IHC of cell pellets from MCF7L-P and TamR, and MCF7L/FOXA1 ± Dox cells. Scale bar, 100 μm. (**b**) Heatmap of differentially expressed genes (|Gfold| > 1.5) after FOXA1 overexpression in MCF7L/FOXA1 cells. The enriched GO terms in DAVID functional annotation of the genes up (440)- or down (217)- regulated upon FOXA1 overexpression (P < 0.001 and P < 0.005, respectively). (**c** and **d**) GSEA shows the correlation of gene expression profile of MCF7L/FOXA1 cells with two gene sets derived from the Endo-R xenograft tumours (P < 0.001). (**e** and **f**) Pearson correlation of FOXA1 mRNA levels and the signature scores of two Endo-R gene sets in ER^+ breast tumours (n = 752). (**g** and **h**) Cell growth was measured in MCF7L/FOXA1 and ZR75-1/FOXA1 cells ± Dox (0.25 or 1 μg ml^{-1}) and treated with endocrine therapy. E2-treated cells were used as normalization controls for anti-oestrogen groups (ED, Tam, and Ful). Data represent means ± SEM. *P < 0.05, **P < 0.01, two-sided t-test for all indicated comparisons.

Figure 4 | *FOXA1* CNG is highly associated with luminal B subtype and a gene signature with prognostic value in ER^+ tumours. (**a**) Box-whisker plots show the *FOXA1*-CN ($\log_2$(CN/2)) across the five molecular subtypes of breast cancer in the TCGA dataset[35]. ****P < 0.0001, Bonferroni post-hoc test (multiple testing corrected). (**b**) Heat map of top 100 differentially expressed genes between ER^+ tumours with *FOXA1*-CNG ($\log_2$(CN/2) > 0.5, n = 70) and tumours without CNG (n = 513). PAM50 subtype annotations are indicated above each tumour. (**c**) Kaplan-Meier plots show the cumulative disease-free survival (DFS) in patients with ER^+ tumours (n = 665) from a breast cancer mega-set[27]. Tumours were stratified into three groups (top one third, intermediate, and bottom one third) according to the calculated FoCAS t-score[37]. Briefly, the t-score was defined for each external profile as the two-sided t-statistic comparing, within the profile, the average of the genes positively associated with *FOXA1*-CNG, with the average of the genes negatively associated with *FOXA1*-CNG. Genes within the dataset were first centered to standard deviations from the median across sample profiles, and only the genes involved in the signature were used in the t-score calculation. P value was

calculated by using log-rank test. (**d**) The same analysis was performed in patients with ER^- tumours (n = 296) from the same mega-set.

Figure 5 | FOXA1 overexpression in ER^+ breast cancer cell lines induces proteomic perturbations in multiple oncogenic signaling pathways. Heat maps of RPPA data representing differentially expressed proteins (one-way ANOVA, $P < 0.05$) in MCF7L/FOXA1 (**a**), ZR75-1/FOXA1 (**b**), and 600MPE/FOXA1 (**c**) cells upon Dox addition for 2 or 5 days. (**d-f**) FOXA1 augmentation-induced signaling perturbations in 14 cancer-related KEGG pathways were evaluated by averaging the expression levels of proteins available from RPPA (numbers in parentheses) within the same pathway, followed by subtraction of basal levels in -Dox cells. A paired one-sided *t*-test was applied and the *P* value was plotted as minus $\log_{10}$-transformed. The perturbations in pathways with $P < 0.05$ ($P = 0.05$ is marked by a dash-line) were statistically significant.

Figure 6 | Integrative analysis revealed *IL8* as a target of increased FOXA1 in ER transcriptional reprogramming. (**a**) Integrated RNA-seq and FOXA1 ChIP-seq data in MCF7L-P and TamR cells. Genes aligned in RNA-seq were calculated for their expression ratio in TamR *vs.* P cells, by which the genes were sorted in a descending order. FOXA1 binding events (tags) within ± 20 kb of each gene's TSS were counted and represented by average normalized RPM (reads per million) for every 300 consecutive genes along the order of expression ratio (TamR/P) from RNA-seq. These FOXA1 tags were plotted separately for P (in blue) and TamR (in red) cells. (**b**) Heat maps of genes with high expression ratio of $\log_2$(TamR/P) > 1.5 and with enriched FOXA1 binding ratio of $\log_{10}$(TamR/P) >1.5. Along these genes, heat map of expression ratio in MCF7L/FOXA1 ± Dox cells is also shown. (**c**) Venn diagram showing the overlap (58), including *IL8*, *BMP7*, and *CTGF* genes, between the FOXA1-overexpression (O.E.) associated genes (440) and the MCF7L-TamR signature genes (428). *P* value was calculated by Fisher's exact test. (**d**) IL-8 gene expression measured by qRT-PCR in four Endo-R cell models. Data represent means ± SEM. $*P < 0.05$, $**P < 0.01$, $***P < 0.001$, two-sided *t*-test for all comparisons between Endo-R and P cells. (**e**) Venn diagram showing the overlaps among the predicted genes with the binding of EGF/E2-stimulated ER or FOXA1 within ± 20 kb of TSS in MCF7 cells. The genes perturbed by FOXA1 overexpression (UP: up-regulated, DN: down-regulated, NA: not altered) were calculated for the enrichment within the gene sets with FOXA1 and EGF-not-E2-stimulated ER

binding (**f**), with FOXA1 and EGF-shared-E2-stimulated ER binding (**g**), and with FOXA1 and E2-not-EGF-stimulated ER binding (**h**). $^{**}P < 0.01$, Fisher's exact test.

Figure 7 | Increased FOXA1 and ER regulate IL-8 expression in ER$^+$ breast cancer. (**a**) Schematic diagram of ER and FOXA1 binding within the *IL8* gene locus as defined by EGF-stimulated ER ChIP-on-chip[41] and FOXA1 ChIP-seq[40] in MCF7 cells. *dis*., distal. *pro*., proximal. (**b**) Snap shot of FOXA1 continuous peaks from ChIP-Seq data showing the binding pattern upstream of *IL8* gene TSS in MCF7L-P and MCF7L-TamR cells treated with Tam or E2. (**c**) FOXA1-ChIP and ER-ChIP followed by qPCR of binding regions in MCF7L-P and TamR cells. Results were quantified by normalization using input DNA. (**d**) Measurement of IL-8 mRNA by qRT-PCR in MCF7L-TamR cells with either ER or FOXA1 knockdown. N.S., non-specific; #1 and #2, two different siRNA sequences. (**e**) IL-8 measurement in 600MPE-TamR cells after ER or FOXA1 knockdown. (**f**) ELISA of IL-8 protein in culture media of MCF7L/FOXA1 -/+Dox cells in the absence/presence of ER knockdown. (**g**) Same measurement in 600MPE/FOXA1 -/+Dox cells as in (**f**). (**h**) Representative H&E staining (Scale bar, 100 μm) and IL-8 IHC images (Scale bar, 50 μm) from E2-treated and Endo-R MCF7L xenograft tumours. (**i**) Scatter dot plots of IL-8 Allred score in (**h**). Data represent means ± SEM. $^{*}P < 0.05$, $^{**}P < 0.01$, $^{***}P < 0.001$, two-sided *t*-test for indicated comparisons. (**j**) Representative IHC images from two ER$^+$ tumours showing low (#1) *vs*. high (#2) FOXA1 and the negative *vs*. positive IL-8 staining, respectively. Scale bar, 50 μm. (**k**) Proportions of positive *vs*. negative IL-8 tumours within the groups of tumours showing the same FOXA1 Allred score (AS). Correlation of IL-8 positivity and FOXA1-AS was evaluated by Fisher's exact test.

Figure 8 | IL-8 mediates the effect of FOXA1 on cell growth and invasion in endocrine resistance. (**a**) Cell growth within 5 days in MCF7L-P and TamR cells with IL-8 knockdown by two different sequences. N.S. knockdown was used as normalization control. (**b**) Cell growth within 5 days in 600MPE-P and TamR cells with IL-8 knockdown using one of the siRNA sequences. (**c**) Western blots of GFR downstream signaling mediators in MCF7L-TamR cells with siRNA knockdown of N.S. or IL-8. (**d**) Measurement of IL-8 and FOXA1 mRNA by qRT-PCR in four MCF7L cell lines stably infected with lentivirus-introduced Dox-inducible overexpression of YFP/FOXA1 and shRNAs of sh-Luc/IL8, in all combinations. (**e**) Cell growth within 7 days

in four MCF7L lines with induction (+Dox, 0.5 μg/ml), treated with E2 (as control) or anti-oestrogen (ED, Tam, and Ful). (**f**) Heatmap of RPPA data (Centered-$\log_2$) of MCF7L/FOXA1 +Dox cells with N.S. or IL-8 knockdown. Shown here is the downregulated signaling in multiple GFR downstream pathways upon IL-8 knockdown. (**g**) Cell invasion measurement in MCF7L-P and TamR cells with N.S. or IL-8 knockdown. Cells were reverse-transfected by siRNA for 48 h and seeded at same number into Matrigel-coated 24-well Transwell plates for additional 12 h. Cell invasiveness was evaluated by counting the invaded cells per well for quadruplicates. (**h**) Same assay as in (**g**) was done in 600MPE-P and TamR cells. (**i**) Cell invasion measurement for MCF7L/FOXA1 cells ± Dox transfected with si-N.S. or si-IL8. (**j**) Same assay as in (**i**) was done in 600MPE/FOXA1 cells. Data represent means ± SEM. *$P < 0.05$, **$P < 0.01$, ***$P < 0.001$, two-sided *t*-test for indicated comparisons.

Supplementary figure legends

Supplementary Fig. S1. Cell growth of multiple Endo-R cell models. (**a-e**) Pre-starved cells culturing with PRF medium and 5% CS-FBS were treated with E2 (control), ED, or Tam for indicated days. Cell numbers were either counted by *in situ* cytometer (Celigo) or quantified with colorimetric assay. **$P < 0.01$, ***$P < 0.001$, unpaired two-sided *t*-test for all the comparisons between E2 treated and anti-oestrogen treated cells.

Supplementary Fig. S2. *FOXA1* amplification in Endo-R cell models. (**a**) Normalized *FOXA1*-CN values from multiple Endo-R cells were calculated from the results of real-time gPCR assay. The normal diploid MCF10A cell line was used as the normalization control (CN = 2, marked by a dashed red line). (**b**) Representative images of bright-field and *FOXA1*-FISH in MCF7RN-P and TamR cells. Scale bar, 100 μm (bright field) and 20 μm (FISH). (**c**) Stacked bar chart summarizes the percentage of cells (n = 65) with *FOXA1*/*REF* foci ratio within indicated ranges. See the supplementary methods for data interpretation.

Supplementary Fig. S3. *FOXA1*-CN in breast cancer cell lines. Normalized *FOXA1*-CN ($\log_2$(CN/2)) across a panel of breast cancer cell lines (n = 59) from the Cancer Cell Line Encyclopedia[22]. Base line (Y axis at 0) indicates the CN of 2. ER^+ cell lines are in red.

Supplementary Fig. S4. Down-regulation of expression of classical ER regulated genes in Endo-R cells. (**a-c**) RPPA assays were performed using cell lysates from three Endo-R cell models. Protein levels were presented as means ± SEM from biologically triplicated samples with triplicated loading dots in the array (n = 9). *P < 0.05, **P < 0.01, ***P < 0.001, unpaired two-sided t-test for all the comparisons between P and Endo-R cells.

Supplementary Fig. S5. Knockdown verification in Endo-R cell models. (**a**) ER and (**b**) FOXA1 knockdown in MCF7L-P and TamR cells was confirmed by Western blots. (**c**) ER and FOXA1 knockdown in 600MPE-TamR cells was verified by qRT-PCR assay. Data represent means ± SEM. **P < 0.01, ***P < 0.001, two-sided t-test for indicated comparisons.

Supplementary Fig. S6. FOXA1 mRNA levels predict outcome in ER$^+$ breast cancer patients receiving endocrine therapy. (**a**) Kaplan-Meier plots show the cumulative RFS in ER$^+$ patients receiving Tam but without chemotherapy (n = 615), who were stratified by FOXA1 mRNA levels at the top quartile (25%) *vs*. the rest (75%). (**b**) Same analysis in ER$^+$ patients without endocrine treatment (n = 500). (**c**) Kaplan-Meier plots show the cumulative distant-metastasis-free survival (DMFS) in ER$^+$ patients receiving endocrine but no chemotherapy (n = 481), who were stratified by FOXA1 mRNA levels at the top quartile (25%) *vs*. the rest (75%). P value was calculated by using the log-rank test. Analysis was performed using an online tool and resource at kmplot.com/analysis[28].

Supplementary Fig. S7. FOXA1 mRNA expression in breast tumours. Box-whisker plots show the FOXA1 mRNA levels (Centered-$\log_2$) across the five molecular subtypes of breast cancer (n = 727) in the TCGA dataset[35]. ****P < 0.0001, Bonferroni post-hoc test (multiple testing corrected).

Supplementary Fig. S8. *FOXA1*-CN is relatively higher in a cohort of breast cancer lymph-node metastases. (**a**) *FOXA1*-CN was derived from a study of whole-genome array-based comparative genomic hybridization (aCGH) (GSE56765)[36]. (**b**) *FOXA1*-CN was compared between primary breast luminal tumours (n = 22) and their matched lymph-node metastases, using the two-tailed paired t-test.

Supplementary Fig. S9. FOXA1 overexpression reduces the protein expression of ER and its classical regulated genes. Bar charts show the protein levels of ER and several ER-regulated genes in MCF7L/FOXA1

cells ± Dox for 2 or 5 days. Protein levels were measured by RPPA and presented as means ± SEM from biologically triplicated samples with triplicated loading dots in the array (n = 9). *P < 0.05, **P < 0.01, ***P < 0.001, unpaired two-sided t-test to compare the expression between +Dox and -Dox cells.

Supplementary Fig. S10. FOXA1 level-dependent effect on the ER and GFR downstream signaling. MCF7L cells with inducible YFP control (**a**) or FOXA1 (**b**) were harvested for protein lysates after 3-days incubation under different doses of Dox. Western blotting was performed using the indicated antibodies. GAPDH blots were used for loading control.

Supplementary Fig. S11. Inverse correlation of proteomic perturbations by FOXA1 alteration in MCF7L-P and TamR cells. (**a**) Heat map of the 89 clustered proteins measured by RPPA that were differentially expressed (one-way ANOVA, P < 0.05) in the MCF7L-TamR cells with FOXA1 *vs*. N.S. (control) knockdown. Arrows indicate the proteins of PR and GATA3. (**b**) Overall comparison of proteomic changes in signaling pathways between the MCF7L/FOXA1 ± Dox cells and the MCF7L-TamR/si-FOXA1 cells. Proteins were assigned to 13 cancer-related pathways defined by KEGG[38]. The sum of all protein signals in each pathway (protein number in parentheses) was averaged and subtracted by that from the controls, representing the pathway perturbations scaled by the left Y-axis. A paired one-sided t-test was applied to assess pathway perturbations in MCF7L/FOXA1 cells with FOXA1 overexpression and MCF7L-TamR cells with FOXA1 knockdown. Minus $\log_{10}$-transformed P value was scaled by the right Y-axis. Gray dash-line marks the P value at 0.05. Pearson correlation was used to assess the concordance of overall proteomic changes between MCF7L-P and TamR cells with corresponding FOXA1 manipulations.

Supplementary Fig. S12. Cistromic profiling of FOXA1 in MCF7L-P and TamR cells. (**a**) Venn diagram showing the overlap of FOXA1 binding events between MCF7L-P and TamR cells. (**b**) Enriched motifs in the differential FOXA1 binding events in MCF7L-P and TamR cells.

Supplementary Fig. S13. Altered ER and PR protein levels in MCF7L Endo-R xenograft tumours. (**a**) Representative ER and PR IHC images from E2-treated and Endo-R MCF7L xenograft tumours. Scale bar, 200 μm. (**b**) Scatter dot plots of ER and PR Allred score in (a). Data represent means ± SEM. **P < 0.01, ***P < 0.001, two-sided t-test for indicated comparisons.

Supplementary Fig. S14. Paranuclear IL-8 staining in cells. MCF7L-P and TamR cells were prepared and processed for IL-8 immunofluorescence staining. DAPI was used for nucleus counterstaining. Scale bar, 100 μm. See the supplementary methods for experiment detail.

Supplementary Fig. S15. Altered gene expression in the MCF7L-TamR cells with FOXA1 or IL-8 knockdown. (a) Heat map of the expression of differentially expressed genes (|Gfold| > 0.5) in the MCF7L-TamR cells with FOXA1 knockdown, aligned with the expression of the same genes in the MCF7L-TamR cells with IL-8 knockdown. (**b**) Pearson correlation of the altered gene expression from (a) (n = 400) due to FOXA1 knockdown and IL-8 knockdown in MCF7L-TamR cells.

Supplementary Fig. S16. IL-8 knockdown rescue assay. A stable MCF7L-TamR/IL-8 cell line was established to express Dox-inducible IL-8, encoded by an *IL8* cDNA without 3'-UTR sequence. Two different *IL8* siRNA sequences, targeting either the *IL8* coding DNA sequence (CDS) (#1) or the 3'-UTR region (#2), were transiently transfected to MCF7L-TamR/IL-8 cells ± Dox at two different doses. A 6-day cell growth measurement was performed using methylene blue staining. Cell growth under N.S. knockdown was used as the normalization control.

Supplementary Fig. S17. Endocrine response in MCF7L stable cell lines with combinations of inducible cDNA or shRNA. Cell growth within 7 days in four MCF7L lines without induction (-Dox), treated with E2 (as control) or anti-oestrogen (ED, Tam, and Ful).

Supplementary Table S1. Enriched gene sets associated with transcriptomic profile of MCF7L cells with FOXA1 overexpression (MSigDB, C6 collection: oncogenic signatures)

Supplementary Table S2. Differentially expressed proteins measured by RPPA between +Dox (at day 2 or 5) and -Dox samples in 3 ER$^+$ cell models (one-way ANOVA, $P < 0.05$).

Supplementary Methods

Kaplan-Meier Curves. Kaplan-Meier analysis was also performed using an online tool of meta-analysis of public microarray datasets[28]. Patients with ER$^+$ tumours (defined by IHC) treated with Tam (without chemo), with systemic treatment (without chemo), or without systemic treatment were included and analyzed for RFS and DMFS between the patients that were stratified by the expression of FOXA1 mRNA at top-quartile level.

Immunofluorescence staining. Cells were grown on poly-L-lysine-coated coverslips (Corning) for 24 h, washed twice in PBS, fixed in 4% formaldehyde, and permeabilized by 0.1% TritonX-100 for 15 min on ice. After blocking in 1% bovine serum albumin (BSA) for 1 h, cells were incubated with IL-8 polyclonal antibody (1:100; Serotec, UK) overnight at 4°C. Immunoreactivity was developed using an anti-rabbit IgG conjugated with Alexa-Fluor-594 (1:500; Cell Signaling) for 1 h at 4°C. Cells were counter-stained in Vectashield mounting medium with DAPI (Vector Laboratories) and then imaged using a Leica confocal imaging system (TCS-SP5) running LAS-AF Application Suite (v1.83).

References

1. Brodie A, Sabnis G. Adaptive changes result in activation of alternate signaling pathways and acquisition of resistance to aromatase inhibitors. *Clin Cancer Res* **17**, 4208-4213 (2011).

2. Ring A, Dowsett M. Mechanisms of tamoxifen resistance. *Endocr Relat Cancer* **11**, 643-658 (2004).

3. Fu X, *et al.* Overcoming endocrine resistance due to reduced PTEN levels in estrogen receptor-positive breast cancer by co-targeting mammalian target of rapamycin, protein kinase B, or mitogen-activated protein kinase kinase. *Breast Cancer Res* **16**, 430 (2014).

4. Creighton CJ, *et al.* Development of resistance to targeted therapies transforms the clinically associated molecular profile subtype of breast tumor xenografts. *Cancer Res* **68**, 7493-7501 (2008).

5. Massarweh S, *et al.* Tamoxifen resistance in breast tumors is driven by growth factor receptor signaling with repression of classic estrogen receptor genomic function. *Cancer Res* **68**, 826-833 (2008).

6. Fu X, Osborne CK, Schiff R. Biology and therapeutic potential of PI3K signaling in ER+/HER2-negative breast cancer. *Breast* **22 Suppl 2**, S12-18 (2013).

7. Clark KL, Halay ED, Lai E, Burley SK. Co-crystal structure of the HNF-3/fork head DNA-recognition motif resembles histone H5. *Nature* **364**, 412-420 (1993).

8. Carroll JS, *et al.* Genome-wide analysis of estrogen receptor binding sites. *Nat Genet* **38**, 1289-1297 (2006).

9. Clarke CL, Graham JD. Non-overlapping progesterone receptor cistromes contribute to cell-specific transcriptional outcomes. *PLoS One* **7**, e35859 (2012).

10. Gao N, *et al.* The role of hepatocyte nuclear factor-3 alpha (Forkhead Box A1) and androgen receptor in transcriptional regulation of prostatic genes. *Molecular endocrinology* **17**, 1484-1507 (2003).

11. Lupien M, *et al.* FoxA1 translates epigenetic signatures into enhancer-driven lineage-specific transcription. *Cell* **132**, 958-970 (2008).

12. Ademuyiwa FO, Thorat MA, Jain RK, Nakshatri H, Badve S. Expression of Forkhead-box protein A1, a marker of luminal A type breast cancer, parallels low Oncotype DX 21-gene recurrence scores. *Modern pathology : an official journal of the United States and Canadian Academy of Pathology, Inc* **23**, 270-275 (2010).

13. Bernardo GM, *et al.* FOXA1 represses the molecular phenotype of basal breast cancer cells. *Oncogene* **32**, 554-563 (2013).

14. West M, *et al.* Predicting the clinical status of human breast cancer by using gene expression profiles. *Proc Natl Acad Sci U S A* **98**, 11462-11467 (2001).

15. Thorat MA, *et al.* Forkhead box A1 expression in breast cancer is associated with luminal subtype and good prognosis. *Journal of clinical pathology* **61**, 327-332 (2008).

16. Badve S, *et al.* FOXA1 expression in breast cancer--correlation with luminal subtype A and survival. *Clin Cancer Res* **13**, 4415-4421 (2007).

17. Mehta RJ, *et al.* FOXA1 is an independent prognostic marker for ER-positive breast cancer. *Breast Cancer Res Treat* **131**, 881-890 (2012).

18. Ross-Innes CS, *et al.* Differential oestrogen receptor binding is associated with clinical outcome in breast cancer. *Nature* **481**, 389-393 (2012).

19. Tangen IL, *et al.* Switch in FOXA1 status associates with endometrial cancer progression. *PLoS One* **9**, e98069 (2014).

20. Zhang Y, Tseng CC, Tsai YL, Fu X, Schiff R, Lee AS. Cancer cells resistant to therapy promote cell surface relocalization of GRP78 which complexes with PI3K and enhances PI(3,4,5)P3 production. *PLoS One* **8**, e80071 (2013).

21. Hiscox S, Morgan L, Green TP, Barrow D, Gee J, Nicholson RI. Elevated Src activity promotes cellular invasion and motility in tamoxifen resistant breast cancer cells. *Breast Cancer Res Treat* **97**, 263-274 (2006).

22. Barretina J, *et al.* The Cancer Cell Line Encyclopedia enables predictive modelling of anticancer drug sensitivity. *Nature* **483**, 603-607 (2012).

23. Feng J, Meyer CA, Wang Q, Liu JS, Shirley Liu X, Zhang Y. GFOLD: a generalized fold change for ranking differentially expressed genes from RNA-seq data. *Bioinformatics* **28**, 2782-2788 (2012).

24. Huang da W, Sherman BT, Lempicki RA. Systematic and integrative analysis of large gene lists using DAVID bioinformatics resources. *Nat Protoc* **4**, 44-57 (2009).

25. Mootha VK, *et al.* PGC-1alpha-responsive genes involved in oxidative phosphorylation are coordinately downregulated in human diabetes. *Nat Genet* **34**, 267-273 (2003).

26. Subramanian A, *et al.* Gene set enrichment analysis: a knowledge-based approach for interpreting genome-wide expression profiles. *Proc Natl Acad Sci U S A* **102**, 15545-15550 (2005).

27. Kessler JD, *et al.* A SUMOylation-dependent transcriptional subprogram is required for Myc-driven tumorigenesis. *Science* **335**, 348-353 (2012).

28. Gyorffy B, *et al.* An online survival analysis tool to rapidly assess the effect of 22,277 genes on breast cancer prognosis using microarray data of 1,809 patients. *Breast Cancer Res Treat* **123**, 725-731 (2010).

29. Deutsch L, *et al.* Opposite roles of FOXA1 and NKX2-1 in lung cancer progression. *Genes Chromosomes Cancer* **51**, 618-629 (2012).

30. Grasso CS, *et al.* The mutational landscape of lethal castration-resistant prostate cancer. *Nature* **487**, 239-243 (2012).

31. Lin L, *et al.* The hepatocyte nuclear factor 3 alpha gene, HNF3alpha (FOXA1), on chromosome band 14q13 is amplified and overexpressed in esophageal and lung adenocarcinomas. *Cancer Res* **62**, 5273-5279 (2002).

32. Nucera C, *et al.* FOXA1 is a potential oncogene in anaplastic thyroid carcinoma. *Clin Cancer Res* **15**, 3680-3689 (2009).

33. Robbins CM, *et al.* Copy number and targeted mutational analysis reveals novel somatic events in metastatic prostate tumors. *Genome Res* **21**, 47-55 (2011).

34. Yasui K, *et al.* Identification of target genes within an amplicon at 14q12-q13 in esophageal squamous cell carcinoma. *Genes Chromosomes Cancer* **32**, 112-118 (2001).

35. Cancer Genome Atlas N. Comprehensive molecular portraits of human breast tumours. *Nature* **490**, 61-70 (2012).

36. Vollebergh MA, *et al.* Lack of genomic heterogeneity at high-resolution aCGH between primary breast cancers and their paired lymph node metastases. *PLoS One* **9**, e103177 (2014).

37. Creighton CJ, *et al.* Insulin-like growth factor-I activates gene transcription programs strongly associated with poor breast cancer prognosis. *J Clin Oncol* **26**, 4078-4085 (2008).

38. Kanehisa M, Goto S. KEGG: kyoto encyclopedia of genes and genomes. *Nucleic Acids Res* **28**, 27-30 (2000).

39. Heiser LM, *et al.* Integrated analysis of breast cancer cell lines reveals unique signaling pathways. *Genome Biol* **10**, R31 (2009).

40. Hurtado A, Holmes KA, Ross-Innes CS, Schmidt D, Carroll JS. FOXA1 is a key determinant of estrogen receptor function and endocrine response. *Nat Genet* **43**, 27-33 (2011).

41. Lupien M, *et al.* Growth factor stimulation induces a distinct ER(alpha) cistrome underlying breast cancer endocrine resistance. *Genes Dev* **24**, 2219-2227 (2010).

42. Singh JK, Simoes BM, Howell SJ, Farnie G, Clarke RB. Recent advances reveal IL-8 signaling as a potential key to targeting breast cancer stem cells. *Breast Cancer Res* **15**, 210 (2013).

43. Britschgi A, *et al.* JAK2/STAT5 inhibition circumvents resistance to PI3K/mTOR blockade: a rationale for cotargeting these pathways in metastatic breast cancer. *Cancer cell* **22**, 796-811 (2012).

44. Chin AR, Wang SE. Cytokines driving breast cancer stemness. *Mol Cell Endocrinol* **382**, 598-602 (2014).

45. Iggo RD WH, Rabbitts P, Quenel-Tueux N, Mauriac L, MacGrogan G, Bonnefoi H. Next generation sequencing shows clonal selection after treatment with anastrozole or fulvestrant in a randomized trial of postmenopausal patients with large operable or locally-advanced hormone-receptor-positive breast cancer. In: *San Antonio Breast Cancer Symposium* (ed^(eds). Cancer Res (2013).

46. Li S, *et al.* Endocrine-therapy-resistant ESR1 variants revealed by genomic characterization of breast-cancer-derived xenografts. *Cell reports* **4**, 1116-1130 (2013).

47. Toy W, *et al.* ESR1 ligand-binding domain mutations in hormone-resistant breast cancer. *Nat Genet* **45**, 1439-1445 (2013).

48. Robinson DR, *et al.* Activating ESR1 mutations in hormone-resistant metastatic breast cancer. *Nat Genet* **45**, 1446-1451 (2013).

49. Jeselsohn R, *et al.* Emergence of constitutively active estrogen receptor-alpha mutations in pretreated advanced estrogen receptor-positive breast cancer. *Clin Cancer Res* **20**, 1757-1767 (2014).

50. Gerhardt J, *et al.* FOXA1 promotes tumor progression in prostate cancer and represents a novel hallmark of castration-resistant prostate cancer. *The American journal of pathology* **180**, 848-861 (2012).

51. Jain RK, Mehta RJ, Nakshatri H, Idrees MT, Badve SS. High-level expression of forkhead-box protein A1 in metastatic prostate cancer. *Histopathology* **58**, 766-772 (2011).

52. Robinson JL, *et al.* Elevated levels of FOXA1 facilitate androgen receptor chromatin binding resulting in a CRPC-like phenotype. *Oncogene* **33**, 5666-5674 (2014).

53. Chin AR, Wang SE. Cytokines driving breast cancer stemness. *Molecular and cellular endocrinology* **382**, 598-602 (2014).

54. Dunbier AK, *et al.* Molecular profiling of aromatase inhibitor-treated postmenopausal breast tumors identifies immune-related correlates of resistance. *Clin Cancer Res* **19**, 2775-2786 (2013).

55. Murphy C, *et al.* Nonapical and cytoplasmic expression of interleukin-8, CXCR1, and CXCR2 correlates with cell proliferation and microvessel density in prostate cancer. *Clin Cancer Res* **11**, 4117-4127 (2005).

56. Morrison G, *et al.* Therapeutic potential of the dual EGFR/HER2 inhibitor AZD8931 in circumventing endocrine resistance. *Breast Cancer Res Treat* **144**, 263-272 (2014).

57. Meerbrey KL, *et al.* The pINDUCER lentiviral toolkit for inducible RNA interference in vitro and in vivo. *Proc Natl Acad Sci U S A* **108**, 3665-3670 (2011).

58. Reich M, Liefeld T, Gould J, Lerner J, Tamayo P, Mesirov JP. GenePattern 2.0. *Nat Genet* **38**, 500-501 (2006).

59. Wang YC, *et al.* Different mechanisms for resistance to trastuzumab versus lapatinib in HER2-positive breast cancers--role of estrogen receptor and HER2 reactivation. *Breast Cancer Res* **13**, R121 (2011).

60. Saldanha AJ. Java Treeview--extensible visualization of microarray data. *Bioinformatics* **20**, 3246-3248 (2004).

61. Creighton CJ, *et al.* Proteomic and transcriptomic profiling reveals a link between the PI3K pathway and lower estrogen-receptor (ER) levels and activity in ER+ breast cancer. *Breast Cancer Res* **12**, R40 (2010).

62. Shin H, Liu T, Manrai AK, Liu XS. CEAS: cis-regulatory element annotation system. *Bioinformatics* **25**, 2605-2606 (2009).

63. Harvey JM, Clark GM, Osborne CK, Allred DC. Estrogen receptor status by immunohistochemistry is superior to the ligand-binding assay for predicting response to adjuvant endocrine therapy in breast cancer. *J Clin Oncol* **17**, 1474-1481 (1999).

FoxA1 gene amplification in ER+ breast cancer mediates endocrine resistance by increasing IL-8

Xiaoyong Fu[1,2,3,4], Rinath Jeselsohn[6], Emporia F. Hollingsworth[5], Dolores Lopez-Terrada[5], Chad J. Creighton[2,3], Agostina Nardone[1,2,3], Martin Shea[1,2,3], Laura M. Heiser[7], Pavana Anur[8], Nicholas Wang[7], Catie Grasso[7], Paul Spellman[8], Carolina Gutierrez[5], Mothaffar F. Rimawi[1,2,3], Susan G. Hilsenbeck[1,2,3], Joe W. Gray[7], Myles Brown[6], C. Kent Osborne[1,2,3,4], Rachel Schiff[1,2,3,4]

[1]Lester and Sue Smith Breast Center, [2]Dan L. Duncan Cancer Center, and Departments of [3]Medicine, [4]Molecular and Cellular Biology, and [5]Pathology, Baylor College of Medicine, Houston, Texas; [6]Dana-Farber Cancer Institute, Harvard Medical School, Boston, Massachusetts; Departments of [7]Biomedical Engineering, and [8]Molecular and Medical Genetics, Oregon Health and Science University, Portland, Oregon

Background: ER transcriptional programming is associated with fundamental changes when endocrine resistance develops. The Forkhead transcription factor, FoxA1, is a pioneer factor for ER-DNA binding. We hypothesize that FoxA1 plays a critical role in ER transcriptional reprogramming in endocrine resistance by augmenting itself and the specific downstream effectors. **Methods:** Next generation sequencing was applied to characterize a panel of endocrine-resistant (Endo-R) cell models. Genomic PCR amplification and FISH assays were developed to measure *FoxA1* copy number gain (CNG). Q-RT-PCR, Western blots, IHC, ELISA, and cytokine arrays were used to determine the levels of FoxA1 and IL-8 in cell culture and *in vivo* xenograft tumors. Effects of gene knockdown (ER, FoxA1, or IL-8) or inducible FoxA1 overexpression on ER and growth factor receptor (GFR) downstream signaling were determined by cell growth and Western blots. ER and FoxA1 binding at the IL-8 gene locus was measured by ChIP-qPCR. ChIP-seq analysis was integrated with RNA-seq data. Kaplan-Meier analysis evaluated the predictive role of FoxA1in ER+ breast tumors. **Results:** Exome-seq revealed that *FoxA1* is the most highly amplified gene in TamR *vs.* P cells from two independent MCF7 models. Genomic PCR and FISH also indicate *FoxA1* CNG in Endo-R models of ZR75-1 and BT474. Increased FoxA1 expression was found in multiple Endo-R cells and in MCF7L Endo-R xenograft tumors. Cytokines, especially IL-8, are more highly expressed in multiple Endo-R cell models, similar to our previous microarray data from MCF7 Endo-R xenograft tumors. FoxA1 forced overexpression significantly induced IL-8 expression in MCF7L-P cells. It also activated multiple GFR downstream signaling pathways, and conferred endocrine resistance. Conversely, knockdown of either FoxA1 or ER significantly decreased IL-8 levels in TamR cells, and inhibited cell growth in both P and TamR cells. Knockdown of IL-8 in TamR cells substantially inhibited GFR downstream signaling, and was more cytotoxic than in P cells. A novel FoxA1-binding site (10 kb at 5'UTR of IL-8) recruited more FoxA1 and p300 in MCF7L-TamR than -P cells. ChIP-seq shows a general enhancement of FoxA1 binding around the genes (within 20 kb) that are differentially expressed in TamR *vs.* P cells. We identified a *FoxA1* CNG-associated gene signature from TCGA breast tumors that predicts worse relapse-free survival (RFS) in Tam-treated ER+ tumors (from Loi et al). Meta-analysis showed that FoxA1 mRNA levels in the top 25th percentile predict worse RFS in ER+ patients treated with Tam (N=615), but not in systemically untreated patients (N=500). FoxA1 CNG and overexpression in clinical specimens by using our newly developed FISH and IHC assays are currently being investigated. **Conclusions:** *FoxA1* gene amplification was enriched in two independent MCF7 Tam-R cell models. Clonal selection of *FoxA1* gene amplification may occur and lead to endocrine resistance. High levels of FoxA1 may mediate endocrine resistance by directly inducing IL-8. The data suggest that IL-8 signaling is a component of a cytokine loop controlled by the FoxA1/ER transcriptional reprogramming, which might be exploited in therapeutics to overcome endocrine resistance.